Circuits and Systems
Mekelweg 4,
2628 CD Delft
The Netherlands
http://ens.ewi.tudelft.nl/

CAS-2018-08

M.Sc. Thesis

Phase Domain Ranging for Narrowband ISM Radio Bands

Aulia Recky Soepeno

Abstract

In this thesis, we study ranging algorithms in an indoor environment using narrow-band industrial, scientific, and medical (ISM) radio bands at 2.4 GHz. Previously, a phase difference approach implemented for this problem. However, the distance estimation is rather inaccurate for indoor ranging, mainly due to multipath and noise. This thesis studies several direction of arrival (DOA) techniques such as matched filter (MF), minimum variance distortionless response (MVDR), and multiple signal classification (MUSIC) to reduce the impact of indoor multipath. Forward-backward smoothing and Akaike information criterion - minimum descriptive length (AIC-MDL) also proposed to diminish the multipath effect further and estimates the number of separable multipath in the channel. Besides, MUSIC-like is discussed to prevent incorrect estimation number of sources. We test the proposed algorithm under different channel parameter value, compensate the bias, and show the performance improvement as the absolute bias value reduced up an order of magnitude.

Phase Domain Ranging for Narrowband ISM Radio Bands

Thesis

submitted in partial fulfillment of the
requirements for the degree of

Master of Science

in

Electrical Engineering

by

Aulia Recky Soepeno
born in Palangkaraya, Indonesia

This work was performed in:

Circuits and Systems Group
Department of Microelectronics & Computer Engineering
Faculty of Electrical Engineering, Mathematics and Computer Science
Delft University of Technology

Delft University of Technology

Delft University of Technology
Department of
Microelectronics & Computer Engineering

The undersigned hereby certify that they have read and recommend to the Faculty of Electrical Engineering, Mathematics and Computer Science for acceptance a thesis entitled **"Phase Domain Ranging for Narrowband ISM Radio Bands"** by **Aulia Recky Soepeno** in partial fulfillment of the requirements for the degree of **Master of Science**.

Dated: 24 August 2018

Chairman: _____
prof. dr. ir. Geert Leus

Advisor: _____
dr. ir. Jac Romme

Committee Members: _____
prof. dr. Alexander Yarovoy

_____

Abstract

In this thesis, we study ranging algorithms in an indoor environment using narrow-band industrial, scientific, and medical (ISM) radio bands at 2.4 GHz. Previously, a phase difference approach implemented for this problem. However, the distance estimation is rather inaccurate for indoor ranging, mainly due to multipath and noise. This thesis studies several direction of arrival (DOA) techniques such as matched filter (MF), minimum variance distortionless response (MVDR), and multiple signal classification (MUSIC) to reduce the impact of indoor multipath. Forward-backward smoothing and Akaike information criterion - minimum descriptive length (AIC-MDL) also proposed to diminish the multipath effect further and estimates the number of separable multipath in the channel. Besides, MUSIC-like is discussed to prevent incorrect estimation number of sources. We test the proposed algorithm under different channel parameter value, compensate the bias, and show the performance improvement as the absolute bias value reduced up an order of magnitude.

Acknowledgements

I would like to thank my advisor prof. dr. ir. Geert Leus for the opportunity and his assistance during the writing of this thesis. I also want to express my gratitude to dr. ir. Jac Romme for his patience, advice, and feedback.

I want to acknowledge Lembaga Pengelola Dana Pendidikan (LPDP) for providing the financial support during my master study. Moreover, this thesis also would not be possible without the support of all my friends and helpful people in the city of Delft that I could not mention one by one.

Nobody has been more important to me in the pursuit of this study than the members of my family. I would like to thank my parents for their endless love and support in whatever I do. I am also immensely indebted to both my new parents in the Netherlands, Richard and Nanda Hettinga. Most importantly, I am grateful to my most supportive partner, Annisa Ika Putri, who always be on my side during the ups-and-downs that I have been through.

Aulia Recky Soepeno
Delft, The Netherlands
24 August 2018

Contents

List of Figures

List of Tables

Glossary

Abbreviations

ACK	Acknowledgement
AGC	Automatic Gain Control
AIC	Akaike Information Criterion
BLE	Bluetooth Low Energy
BW	Bandwidth
CDF	Cumulative Distribution Function
CIR	Channel Impulse Response
CS	Compressed Sensing
CSI	Channel State Information
CW	Continuous Wave
DOA	Direction of Arrival
DOF	Degrees of Freedom
EM	Electromagnetics
EVD	Eigenvalue Decomposition
FB	Forward-backward
FBS	Forward-backward Smoothing
GNSS	Global Navigation Satellite System
GPS	Global Positioning System
ISM	Industrial, Scientific, and Medical
LCMV	Linearly Constrained Minimum Variance
LOS	Line of Sight
MDL	Minimum Description Length
MF	Matched Filter
ML	Maximum Likelihood
MPC	Multipath Component
MUSIC	Multiple Signal Classification
MVDR	Minimum Variance Distortionless Response
NB	Narrowband
NLOS	Non-line of Sight
PDF	Probability Density Function
PDP	Power Delay Profile
PLL	Phase-locked Loop
RSSI	Received Signal Strength Indicator
SFD	Start Frame Delimiter
SH	Sequential Hypothesis
SNR	Signal to Noise Ratio
SS	Spatial Smoothing
SVD	Singular Value Decomposition
TOA	Time of Arrival
UWB	Ultra-wideband

Notations

a	Single element
$\mathbf{a}$	Vector
$\mathbf{A}$	Matrix
$\mathbf{I}$	Identity matrix
$\mathbf{A}^*$	Conjugate of $\mathbf{A}$
$\mathbf{A}^{\mathrm{T}}$	Transpose of $\mathbf{A}$
$\mathbf{A}^{\mathrm{H}}$	Complex conjugate transpose of $\mathbf{A}$
$\mathbf{A}^{-1}$	Inverse of $\mathbf{A}$
$\lvert\mathbf{A}\rvert$	Determinant of $\mathbf{A}$
mod(.)	Modulo operation

1 Introduction

In this thesis, we study algorithms for phase-based ranging in an indoor environment using narrow-band industrial, scientific, and medical (ISM) radio bands at 2.4 GHz.

1.1 Background

High-accuracy localization is essential for mobile users, industrial applications, and warehouses. An excellent location sensing system allows a mobile device to determine its position correctly. Then, various location-based services, for instance in tracking, navigating, and monitoring, would be possible for this device [3]. Therefore, ranging and localization is a key for radio networks.

The global positioning system (GPS) is the most widely used positioning system in the world, based on global navigation satellite system (GNSS) [4]. However, GPS is not compatible for indoor use, because of line of sight (LOS) transmission between receivers and satellites is not feasible in an indoor environment. The indoor environment is more complicated compared to outdoor, due to various additional obstacles, such as walls, equipment, or human. These obstacles affect the propagation of electromagnetic (EM) waves, which lead to multipath. Multipath, along with noise, deteriorates the accuracy of positioning.

There are several approaches to gather range information from radio networks for indoor location and these approaches are based on the positioning algorithm [5]. Time of arrival (TOA) and received signal strength indicator (RSSI) are some examples of range information [6, 7].

This project will be conducted based on the phase difference approach, which is an indirect TOA. Several reasons for using this approach are [2]:

1. Suitable for multipath environments
2. It can be implemented using low-cost components
3. It is well known that using ultra-wideband (UWB), accurate indoor ranging can be realized. Due to its broad bandwidth, a temporal resolution is accomplished with the ability to separate LOS from multipath reflections. However, UWB technology is not compatible with that of popular radio communication technology like Bluetooth low energy (BLE) and Zigbee. Therefore, we focus on the phase-difference approach, which can be realized using a narrowband BLE/Zigbee transceiver [8].

1.2 Motivation

The main problem in indoor ranging is multipath propagation. The existence of multipath, which gives both constructive and destructive interference to the signal, produces

uncertainties in the TOA estimate. It is possible since the direct path is not always the fastest and strongest one. This situation leads to important consequences, such as a significant ranging bias [9].

There is also another problem with a narrow-band measurement, which is around 2 MHz bandwidth (BW). This measurement is very vulnerable to the multipath channel in consequence of possibility out-of-phase addition between LOS and non-line of sight (NLOS) waveforms. A narrower-band frequency means a longer pulses durations. Thus, it is more sensitive to multipath effect. The reflected pulse has a big chance to collide with the LOS pulse and lead to deteriorating the signal because the transmission duration of the narrow-band pulse is around 500 ns for 2 MHz BW [10].

Based on the main issue above, the phase difference approach requires to carry out its ranging measurements at multiple tones/frequencies, to alleviate the multipath effect. The idea is merely to gather the information from a frequency band as wide as possible, where it is around 80 MHz for a 2.4 GHz ISM band. The number of tones/frequencies used can be selected depending on the severity of multipath propagation, which can be seen based on the ratio of LOS signal power to signal power in delay paths, or Rician K-factor [11].

1.3 Problem statement

Based on the background and motivation mentioned in the above section, there are three main problems which summarize the content of this thesis. The first problem is to improve the result of ranging accuracy of phase differences using advanced estimation methods derived from direction of arrival (DOA) algorithms. The second problem is to distinguish and resolve the number of separable multipath among all possible multipath components. The performance of this algorithm is re-evaluated within the same environment after compensating the bias.

1.4 Thesis outline

The rest of this thesis is organized as follows. Chapter 2 gives the necessary background of the phase difference ranging model and its compliance with IEEE 802.15.4, the theory of ranging algorithm based on DOA, and related topics. In Chapter 3, the proposed ranging algorithms are presented alongside with simulation results. Chapter 4 introduces the bias compensation to improve the ranging accuracy further. Chapter 5 introduce a variation of ranging algorithms which are not based on requiring a-priori knowledge of source number while maintaining the performance under adverse channel conditions. Chapter 6 concludes the project and suggests future work.

2 Theoretical Backgrounds

2.1 Phase difference

Phase difference is a ranging technique in which the mean of the signal phase shift is used to measure signal propagation. The ranging scheme is based on the active reflector principle as shown in Figure 2.1.

Device A transmits a continuous wave (CW) signal modeled by $\sin 2\pi ft$. Device B receives the CW signal by a certain phase shift due to the distance r and the radio propagation.

The active reflector principle allows only half duplex operation. This principle means that both devices A and B may not communicate in both directions simultaneously. In this principle, both devices A and B establish phase measurements. The received phase at the receiver ϕ_0 can be expressed as a function of the wavelength of frequency f_0. Both the initiator (A) and reflector (B) devices have a clock reference and are coarsely synchronized to each other, with a time bias of Δt:

$$\phi_{0_{AB}} = 2\pi f_0(\frac{r}{c} - \Delta t) \mod 2\pi \qquad \phi_{0_{BA}} = 2\pi f_0(\frac{r}{c} + \Delta t) \mod 2\pi \tag{2.1}$$

Device B measures the incoming signal phase $\phi_{0_{AB}}$ and compares this phase to the local oscillator (LO) signal phase. Device B transfers back the phase difference to device A, resulting in $\phi_{0_{BA}}$, and uses it as a correction factor:

$$\phi_0 = \phi_{0_{AB}} + \phi_{0_{BA}} = 4\pi f_0(\frac{r}{c}) \mod 2\pi \tag{2.2}$$

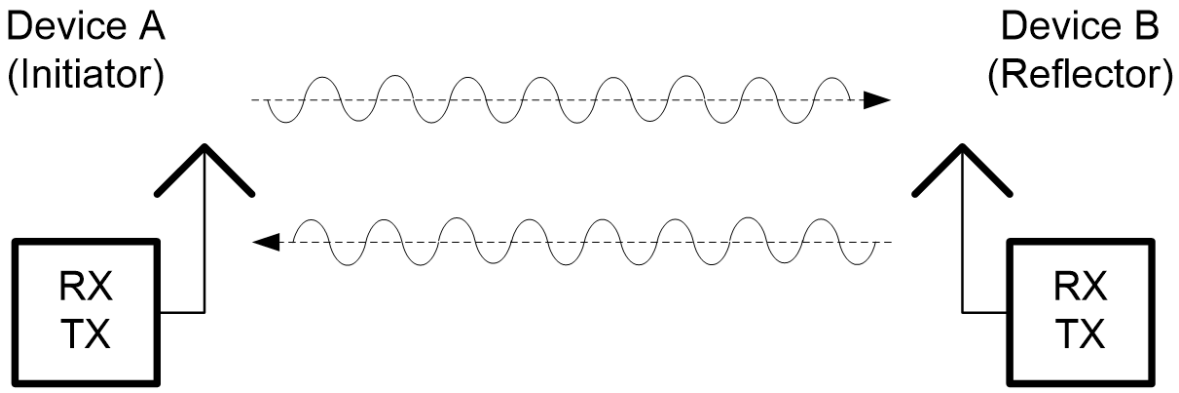

Figure 2.1: Active reflector principle [1]

Another phase measurement on a second frequency $f_1 = f_0 + \Delta f$, gives ϕ_1, where $\Delta\phi = \phi_1 - \phi_0$ is given by:

$$\Delta\phi = \phi_1 - \phi_0 = 4\pi\Delta f\frac{r}{c} \mod 2\pi \tag{2.3}$$

with

$$r = \frac{c}{4\pi\Delta f}\Delta\phi \mod \frac{c}{2\Delta f} \tag{2.4}$$

and the maximum distance (maximum unambiguous range) can only count up to $d_{max} = \frac{c}{2\Delta f}$.

This phase measurement is done in the 2.4 GHz ISM band based on active reflector principle. In fact, two frequencies are adequate to calculate a distance with the phase difference technique, whereas this measurement uses a large number of phase values which is obtained in uniform frequency steps. This method is beneficial to recognize and negate small-band interferences on specific frequencies and to manage the measurement unpredictabilities on the hardware level. Therefore, these multi-tones, with uniform frequency steps of Δf MHz over the entire ISM band, calculate K_f measurement points from ϕ_0 to ϕ_{K_f-1} and K_f energy measurements from each frequency.

K_f phase measurements show the number of tones used in this project. If $\Delta f = \Delta$ MHz, and the bandwidth is B MHz, then $B = (K_f - 1)\Delta$. Implicitly, the number of tones is $K_f = \frac{B+\Delta}{\Delta}$. Also, measuring all K_f tones from ϕ_0 to ϕ_{K_f-1} means that there are $K_f - 1$ measurement point differences, $\Delta\phi_1 \ldots \Delta\phi_{K_f-1}$. Thus, we calculate the average value of the measurement point $\Delta\phi$ as:

$$\Delta\phi = \frac{1}{K_f - 1}\sum_{i=1}^{K_f-1}\Delta\phi_i \tag{2.5}$$

Figure 2.2 illustrates that the ranging procedure using phase measurements in this thesis, with a more detailed ranging sequence shown in Table 2.1. In general, device A begins the ranging measurement. Device B executes a range measurement while device A transmits a carrier, and vice-versa. Device B sends a frame with measurement results to device A, before device A can determine the range between A and B. We may also measure the magnitude of the channel, which combined with the phase gives the measurement of $H(f)$, which allows for more advanced signal processing techniques.

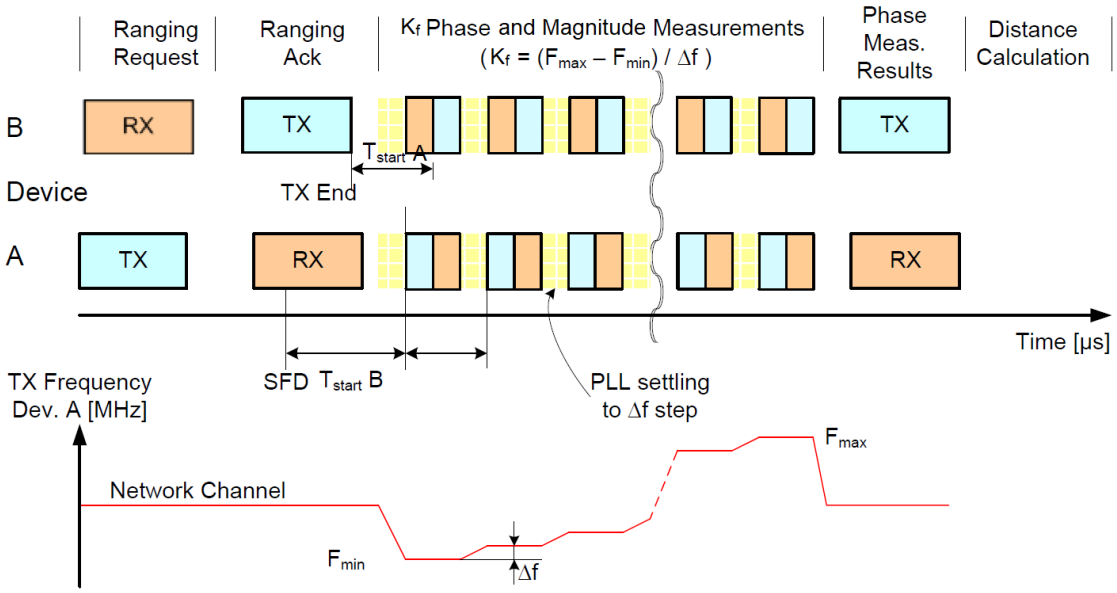

Figure 2.2: Ranging procedure [2]

Table 2.1: Ranging sequence[2]

No	Device A	No	Device B
1	Transmit ranging request frame		
		1	Lock automatic gain control (AGC) after receive request frame
		2	Transmit ranging acknowledgement (ACK)
2	Receive ranging ACK		
3	Lock AGC		
4	Starting timer after Rx end	3	Starting timer after Tx end
5	Setting phase-locked loop (PLL) to 1st measurement frequency		
6	Starting phase measurement sequence		
		4	Setting PLL to 1st measurement frequency
7	Setting PLL to original frequency		
		5	Starting phase measurement sequence
		6	Setting PLL to original frequency
		7	Transmit result frame
8	ACK result frame		
		8	Receive ACK
		9	Release AGC lock
9	Release AGC lock		
10	Restore IF position		
11	Distance calculation		

2.2 Channel model

In general, the channel can be presented by its low-pass channel impulse response $h(t)$ as follows [12]:

$$h(t) = \sum_k \beta_k e^{j\theta_k} \delta(t - \tau_k) \tag{2.6}$$

where $\delta(.)$ is the Dirac delta function and parameters of the k-th path β_k, τ_k, and θ_k are the real positive gain, propagation delay, and phase shift, respectively. j is the

imaginary unit, defined by $\sqrt{-1}$. The Fourier transform of channel impulse response is:

$$H(f) = \int_{-\infty}^{\infty} h(t) e^{-j2\pi ft}\, dt = \sum_k \beta_k e^{-j2\pi f\tau_k + j\theta_k} \tag{2.7}$$

With a uniform frequency step between each tone, in example $f_i = f_{i-1} + \Delta f = f_c + i\Delta f$, the frequency response becomes:

$$\begin{aligned} H(f_i) = h_i &= \sum_k \beta_k e^{-j2\pi f_i \tau_k + j\theta_k} \qquad i = 0, 1, \ldots, K_f - 1 \\ &= \sum_k \beta_k e^{-j2\pi (f_c + i\Delta f)\tau_k + j\theta_k} \\ &= \sum_k \beta_k e^{-j2\pi (f_c\tau_k + i\Delta f\tau_k - \theta_k)} \\ &= \sum_k \beta_k e^{j\theta_k} e^{-j2\pi\tau_k (f_c + i\Delta f)} \\ &= \sum_k \underbrace{\beta_k e^{j\theta_k - j2\pi\tau_k f_c}}_{a_k} \underbrace{e^{-j2\pi\tau_k i\Delta f}}_{z_k} \end{aligned} \tag{2.8}$$

Note that k in principle extends from 0 to ∞. However, in our simulation model, it is truncated from 1 to N_p. Also, i shows the tone index and f_c is around 2.4 GHz.

β_k, τ_k, and θ_k are random parameters due to the people motion and equipment in and around the building. Nevertheless, these parameters can be assumed as virtually invariant random variables as we assume that the channel is virtually slow.

Turin first suggested the formulation in (2.8) as statistical modeling of the urban radio channel [13]. This model was later used for statistical modeling of the indoor radio channel [14, 15, 16], which was first introduced by Saleh and Valenzuela at Bell Laboratories as the earliest statistical modeling of the multipath profiles for the indoor radio channel [17]. The IEEE 802.11 and IEEE 802.15 community referred to these models above to build practical models. They used all of them to compare the evaluation performance of various possible implementations [18].

The channel model from this ranging procedure is based on the Saleh-Valenzuela non-cluster model [17]. This model is a method to generate model realizations [19]. The channel model aims to get the joint statistics of arrival times and path gains (τ_k, β_k), respectively, as defined in (2.8). The phase angles, θ_k, will be assumed to be statistically independent random variables with a distribution over $[0, 2\pi]$.

This channel model in its simplest form assumes that the magnitude of all paths after LOS follow a Rayleigh distribution, the arrival time of the paths forms a Poisson random variable, and the envelope of the power delay spectrum forms an exponentially decaying function. Under this model, the proposed LOS propagation time, τ_0, equals:

$$\tau_0 = \frac{r}{c} \tag{2.9}$$

where c is the speed of light and r is the separation distance between transmitter and receiver as explained in Section 2.1.

Actually, according to this model, multipath arrivals happen in clusters. Clusters arrive according to a Poisson arrival process with fixed rate μ. However, in our case, we simplified this model as we do not consider clusters except for one. Therefore, we only consider the arrival of multipath rays also according to a Poisson process with a fixed rate Λ.

The inter-arrival times between each ray are distributed exponentially since the arrival process is Poisson. If τ_k denotes the kth ray arrival, with $k = 0, 1, 2, ...$, the probability density functions (PDF) will be:

$$p(\tau_k \mid \tau_{k-1}) = \Lambda \exp[-\Lambda(\tau_k - \tau_{k-1})], \quad k > 0 \tag{2.10}$$

and the power delay profile (PDP) can be expressed using β_k^2, which is a negative exponential function of τ_k:

$$\begin{aligned} \overline{\beta_k^2} &\equiv \overline{\beta^2(\tau_k)} \\ &= \overline{\beta^2(0)}\ e^{-\tau_k/\gamma} \end{aligned} \tag{2.11}$$

where $\overline{\beta^2(0)} = \overline{\beta_0^2}$ is the average power gain at delay 0. The parameter γ is the ray power-delay time constant. PDP gives the intensity distribution of a signal received through a multipath channel as a function of propagation delay. The propagation delay is the difference in travel time between multipath arrivals.

A Rician K-Factor is also an important parameter used to characterize the PDP, defined as a ratio between LOS and non-LOS (NLOS) delay:

$$K = \frac{\beta^2}{2\sigma^2} \tag{2.12}$$

with $2\sigma^2$ the mean power of the scattered paths. Figure 2.3 shows an example of a channel impulse response and power delay profile for this channel model simulation.

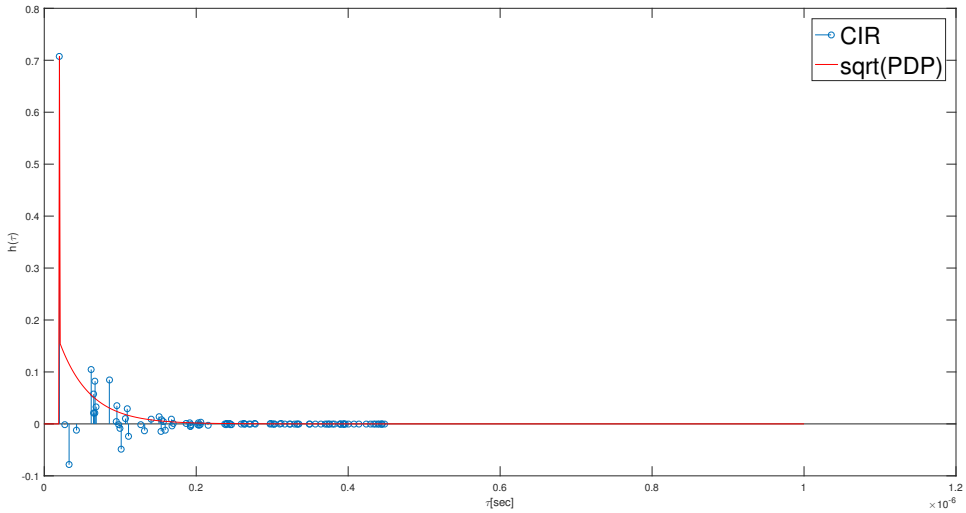

Figure 2.3: Channel Impulse Response (CIR) and Power Delay Profile (PDP) K-factor = 1, $\Lambda = 0.25$ [1/ns]. It is the parameter used for the majority of our simulations

2.3 Ranging algorithms based on channel magnitudes

Phase difference as explained in Section 2.1, is useful enough as a ranging method for a single ray channel, which is a pure LOS. However, our channel model is derived from the multi-ray model. It is more accurate to model the real-life indoor situations, where there is a lot of multipath coming to the receiver. Therefore, a combination of an advanced signal processing algorithm is needed to reduce the impact of multipath. However, the information of channel magnitudes is required as well instead of just channel phase measurements. Nevertheless, the measurement of channel magnitudes can be easily obtained using a narrowband (NB) transceiver.

First, for the noiseless case, the channel vector is obtained from a set of selected frequencies. In this case, we have K_f tones in the ISM Band. Therefore, it will result into:

$$\mathbf{h} = \begin{bmatrix} h_0 \\ h_1 \\ h_2 \\ \vdots \\ h_{K_f-1} \end{bmatrix} = \begin{bmatrix} 1 & 1 & \dots & 1 \\ z_0 & z_1 & \dots & z_{N_p-1} \\ z_0^2 & z_1^2 & \dots & z_{N_p-1}^2 \\ \vdots & \vdots & \ddots & \vdots \\ z_0^{K_f-1} & z_1^{K_f-1} & \dots & z_{N_p-1}^{K_f-1} \end{bmatrix} \begin{bmatrix} a_0 \\ a_1 \\ \vdots \\ a_{N_p-1} \end{bmatrix} \tag{2.13}$$

where z_k is equal to $e^{-j\tau_k \Delta f}$ and $a_k = \beta_k e^{j\theta_k - j\tau_k f_c}$.

To obtain a MUSIC algorithm, we initially converted this channel vector into a

$(L+1) \times (K_f - L)$ Hankel matrix, $\mathbf{H}$[20]:

$$\mathbf{H} = \begin{bmatrix} h_0 & h_1 & \dots & h_{K_f-L-1} \\ h_1 & h_2 & \dots & h_{K_f-L} \\ \vdots & \vdots & \ddots & \vdots \\ h_L & h_{L+1} & \dots & h_{K_f-1} \end{bmatrix} \tag{2.14}$$

$$= \begin{bmatrix} \mathbf{Za} & \mathbf{ZD(z)}^1\mathbf{a} & \dots & \mathbf{ZD(z)}^{K_f-L-1}\mathbf{a} \end{bmatrix} \tag{2.15}$$

$$= \mathbf{Z} \begin{bmatrix} \mathbf{a} & \mathbf{D(z)}^1\mathbf{a} & \dots & \mathbf{D(z)}^{K_f-L-1}\mathbf{a} \end{bmatrix} \tag{2.16}$$

with

$$\mathbf{Z} = \begin{bmatrix} 1 & 1 & \dots & 1 \\ z_0 & z_1 & \dots & z_{N_p-1} \\ z_0^2 & z_1^2 & \dots & z_{N_p-1}^2 \\ \vdots & \vdots & \ddots & \vdots \\ z_0^L & z_1^L & \dots & z_{N_p-1}^L \end{bmatrix} \qquad \mathbf{a} = \begin{bmatrix} a_0 \\ a_1 \\ \vdots \\ a_{N_p-1} \end{bmatrix} \tag{2.17}$$

with $\mathbf{Z}$ is a $(L+1) \times N_p$ matrix with a Vandermonde structure and vector $\mathbf{a}$ has size of $N_p \times 1$, and creates $\mathbf{H}$ using a form of smoothing [21]. $\mathbf{D(z)}^i$ is a Diag operator which is defined as:

$$\mathbf{D(z)}^i = \begin{bmatrix} z_0^i & 0 & 0 & \dots & 0 \\ 0 & z_1^i & 0 & \dots & 0 \\ 0 & 0 & z_2^i & \dots & 0 \\ \vdots & \vdots & \vdots & \ddots & \vdots \\ 0 & 0 & 0 & \dots & z_{N_p-1}^i \end{bmatrix} \tag{2.18}$$

Smoothing is a technique firstly introduced in the spatial processor to eliminate the singularity in both the input signal and interference correlation matrix. This singularity was created by the coherence between the desired signal and the interference. Evans et al. [22] initially used spatial smoothing (SS) in the direction-finding problem. Shan and Kailath [23] modified it to the beamforming problem.

Looking at (2.20), the channel vector $\mathbf{h}$ is indexed from 0 to $K_f - 1$. We construct a set of $K_f - L$ subvectors of length $L + 1$. Each subvector is shifted by one from the previous subvector. The ith subvector has the ith element as its first element. In other words, we can see the channel vector $\mathbf{h}$ is now divided into overlapping subvectors of size $L+1$ that form the first subvector of $\{h_0, \dots, h_L\}$, second subvector of $\{h_1, \dots, h_{L+1}\}$, until the last, $(K_f - L)$th, subvector of $\{h_{K_f-L-1}, \dots, h_{K_f-1}\}$.

Unlike a covariance matrix, the Hankel matrix might not be squared. Therefore, we attempt to make it square by multiplying it with its Hermitian:

$$\overline{\mathbf{H}} = \mathbf{H}\mathbf{H}^{\mathrm{H}} \tag{2.19}$$

which creates a new squared matrix of size $(L + 1) \times (L + 1)$. $\overline{\mathbf{H}}$ has a structure as Hermitian matrix.

The algorithm process will be slightly different in case of the noise present as:

$$\mathbf{h} = \begin{bmatrix} h_0 \\ h_1 \\ h_2 \\ \vdots \\ h_{K_f-1} \end{bmatrix} = \begin{bmatrix} 1 & 1 & \dots & 1 \\ z_0 & z_1 & \dots & z_{N_p-1} \\ z_0^2 & z_1^2 & \dots & z_{N_p-1}^2 \\ \vdots & \vdots & \ddots & \vdots \\ z_0^{K_f-1} & z_1^{K_f-1} & \dots & z_{N_p-1}^{K_f-1} \end{bmatrix} \begin{bmatrix} a_0 \\ a_1 \\ \vdots \\ a_{N_p-1} \end{bmatrix} + \begin{bmatrix} n_0 \\ n_1 \\ n_2 \\ \vdots \\ n_{K_f-1} \end{bmatrix} \tag{2.20}$$

with $n_i \sim \mathcal{N}(0, \sigma^2)$ here is the noise added in each tone. The Hankel matrix $\mathbf{H}$ also contains some noise now:

$$\mathbf{H} = \begin{bmatrix} h_0 & h_1 & \dots & h_{K_f-L-1} \\ h_1 & h_2 & \dots & h_{K_f-L} \\ \vdots & \vdots & \ddots & \vdots \\ h_L & h_{L+1} & \dots & h_{K_f-1} \end{bmatrix} = \begin{bmatrix} \mathbf{Za} & \mathbf{ZD(z)}^1\mathbf{a} & \dots & \mathbf{ZD(z)}^{K_f-L-1}\mathbf{a} \end{bmatrix} + \mathbf{N} \tag{2.21}$$

and

$$\mathbf{N} = \begin{bmatrix} n_0 & n_1 & \dots & n_{K_f-L-1} \\ n_1 & n_2 & \dots & n_{K_f-L} \\ \vdots & \vdots & \ddots & \vdots \\ n_L & n_{L+1} & \dots & n_{K_f-1} \end{bmatrix} \tag{2.22}$$

After this, the next few sections will present a short overview of different ranging estimation algorithms. In general, these algorithms can be divided into two classes: conventional techniques and subspace techniques.

The conventional techniques are based on digital beamforming in DOA algorithms, and they require a large number of tones to achieve a high resolution. These techniques electronically steer beams in all possible delays and look for the first significant peak in the output power. Matched Filter and Minimum Variance Distortionless Response (MVDR) belong to this category.

2.3.1 Matched Filter

One of the most straightforward conventional techniques is Matched Filter (MF), where the time uncertainty region is scanned and a power measurement is taken for all delays [24, 25]. A matched filter estimates the LOS delay by choosing the one that maximizes the output power while scanning over all possible τ:

$$\hat{P}_{MF}(\tau) = \mathbf{e}(\tau)^{\mathrm{H}}\overline{\mathbf{H}}\mathbf{e}(\tau), \tag{2.23}$$

where $\mathbf{e}(\tau)$ is the steering vector defined as:

$$\mathbf{e}(\tau) = \begin{bmatrix} 1 \\ e^{-j2\pi\Delta_f\tau} \\ e^{-j2\pi 2\Delta_f\tau} \\ \vdots \\ e^{-j2\pi L\Delta_f\tau} \end{bmatrix} \tag{2.24}$$

The distance estimation using this method is obtained from the earliest notable peak among all visible peaks.

2.3.2 MVDR

The MVDR technique was initially introduced by Capon in 1969 and is also known as Capon's method, linearly constrained minimum variance (LCMV), or maximum likelihood method.

This algorithm minimizes the output power while constraining the energy towards the delay τ [26]. This minimization is done conditionally so that the gain at the delay of the estimated LOS value is kept constant, meaning the signal is passed without distortion:

$$\hat{\tau} = \max_{\tau}{}_1\{\min_{\mathbf{w}} \mathbf{w}^{\mathrm{H}}\overline{\mathbf{H}}\mathbf{w} \qquad \text{subject to} \qquad \mathbf{w}^{\mathrm{H}}\mathbf{e}(\tau) = 1\} \tag{2.25}$$

where the operator $\max_1$ means the first local maximum and $\mathbf{w}$ is the $(L+1) \times 1$ complex vector. The weight coefficient vector of the MVDR algorithm can be solved using Lagrangian multipliers. Lagrangian multipliers are designated to optimize a multivariable function subject to one or several constraints. The Lagrangian function then can be arranged as:

$$L(\mathbf{w}, \lambda) = \mathbf{w}^{\mathrm{H}}\overline{\mathbf{H}}\mathbf{w} - \lambda(\mathbf{w}^{\mathrm{H}}\mathbf{e}(\tau) - 1) \tag{2.26}$$

where λ is the Lagrange multiplier. Setting the derivatives of (2.26) with respect to $\mathbf{w}$ equal to zero yields:

$$\begin{aligned} \frac{dL(\mathbf{w}, \lambda)}{d\mathbf{w}} &= \overline{\mathbf{H}}\mathbf{w} - \lambda\mathbf{e}(\tau) = \mathbf{0} \\ \mathbf{w} &= \lambda\overline{\mathbf{H}}^{-1}\mathbf{e}(\tau) \end{aligned} \tag{2.27}$$

Both sides of (2.27) can be multiplied by $\mathbf{e}(\tau)^{\mathrm{H}}$, which the left-hand side is equal to 1 based on (2.25). The value of λ is then equal to $\{\mathbf{e}(\tau)^{\mathrm{H}}\overline{\mathbf{H}}^{-1}\mathbf{e}(\tau)\}^{-1}$. Substitutes back the value value of λ to (2.27), we obtains:

$$\mathbf{w} = \frac{\overline{\mathbf{H}}^{-1}\mathbf{e}(\tau)}{\mathbf{e}(\tau)^{\mathrm{H}}\overline{\mathbf{H}}^{-1}\mathbf{e}(\tau)} \tag{2.28}$$

The output power is given by:

$$\hat{P}_{MVDR}(\tau) = \frac{1}{\mathbf{e}(\tau)^{\mathrm{H}}\overline{\mathbf{H}}^{-1}\mathbf{e}(\tau)} \tag{2.29}$$

Hence, we will solve:

$$\hat{\tau} = \max_{\hat{\tau}}{}_1 \ \hat{P}_{MVDR}(\tau) \tag{2.30}$$

2.3.3 MUSIC + Smoothing

Most of the conventional techniques have resolution limitations because they do not exploit the eigenstructure of the Hankel matrix. Subspace-based methods, such as MUSIC, utilize this structure and make it possible to find a high-resolution algorithm.

Therefore, we first compute the singular value decomposition (SVD) of $\mathbf{H}$:

$$\mathbf{H} = \mathbf{U}\boldsymbol{\Sigma}(\mathbf{s})\mathbf{V}^{\mathrm{H}} \tag{2.31}$$

In the noiseless case, the MUSIC algorithm can then be obtained by applying eigenvalue decomposition (EVD) of $\overline{\mathbf{H}}$:

$$\overline{\mathbf{H}} = \mathbf{U}\boldsymbol{\Sigma}(\mathbf{s})\mathbf{V}^{\mathrm{H}}\mathbf{V}\boldsymbol{\Sigma}(\mathbf{s})\mathbf{U}^{\mathrm{H}} \tag{2.32}$$

$$\overline{\mathbf{H}} = \mathbf{U}(\boldsymbol{\Sigma}(\mathbf{s}))^2\mathbf{U}^{\mathrm{H}} \tag{2.33}$$

$$\overline{\mathbf{H}} = \mathbf{U}(\boldsymbol{\Sigma}(\mathbf{s}))^2\mathbf{U}^{\mathrm{H}} = \begin{bmatrix}\mathbf{U_s} & \mathbf{0}\end{bmatrix}\begin{bmatrix}\mathbf{\Sigma_s}^2 & \mathbf{0} \\ \mathbf{0} & \mathbf{0}\end{bmatrix}\begin{bmatrix}\mathbf{U_s}^{\mathrm{H}} & \mathbf{0}^{\mathrm{H}}\end{bmatrix} \tag{2.34}$$

The pseudo-spectrum now looks like:

$$\hat{P}_{MU}(\tau) = \frac{1}{\sum_{i=1}^{L+1} |\mathbf{e}(\tau)^{\mathrm{H}}\mathbf{u}_i|} \tag{2.35}$$

with $\mathbf{U} = [\ \mathbf{u}_1|\ldots|\mathbf{u}_{L+1}]$. In the ranging context, we may exactly find the first significant peak based on all peaks shown in the pseudo-spectrum.

In the noisy case, since there is no a priori information related to how many sources we have, the vector space $\mathbf{U}$ is divided into the signal and the noise subspace by an assumed number of N_s and $L+1-N_s$, respectively, with $N_s \leq L+1$. In MATLAB, the default value of N_s is equal to half of $L+1$.

$$\overline{\mathbf{H}} = \mathbf{U}(\boldsymbol{\Sigma}(\mathbf{s}))^2\mathbf{U}^{\mathrm{H}} = \begin{bmatrix}\mathbf{U_s} & \mathbf{U_n}\end{bmatrix}\begin{bmatrix}\mathbf{\Sigma_s}^2 & \mathbf{0} \\ \mathbf{0} & \mathbf{\Sigma_n}^2\end{bmatrix}\begin{bmatrix}\mathbf{U_s}^{\mathrm{H}} & \mathbf{U_n}^{\mathrm{H}}\end{bmatrix} \tag{2.36}$$

In this case, if the steering vector is almost orthogonal to the noise subspace, a multipath component (MPC) is found. Steering vectors corresponding to the possible delays of arriving signal lie in the signal subspace and are consequently orthogonal to the noise subspace. The LOS delay can be determined by looking through all possible array steering vectors to get those which are orthogonal to the space spanned by the noise vector.

Hence, the pseudo-spectrum becomes [27]:

$$\hat{P}_{MU}(\tau) = \frac{1}{\sum_{i=\frac{L+1}{2}}^{L+1} |\mathbf{e}(\tau)^{\mathrm{H}}\mathbf{u}_i|} \tag{2.37}$$

Range estimation can now be derived based on this pseudo-spectrum by finding the first significant peak among all peaks shown.

Smoothing is beneficial for this ranging estimation since the signal is partially correlated due to the multipath propagation. By using smoothing, it needs $2K$ number of measurements to solve K correlated signals.

3 Proposed Method

In this chapter, we continue the study from Chapter 2 by comparing the results between MF, MVDR, and MUSIC. After that, three main different possible structures of $\mathbf{H}$ in order to create a squared $\overline{\mathbf{H}}$ matrix are also reviewed. Then, we propose an approach to reduce the multipath effect based on an incorporated eigenstructure-based technique of $\overline{\mathbf{H}}$, called as forward-backward smoothing (FBS) and an information theory based techniques, namely Akaike Information Criterion (AIC) and Minimum Description Length (MDL).

3.1 Channel parameter

Six different parameters such as LOS delay, K-Factor, ray interval rate, ray decay constant, SNR, and number of tones were applied in the simulation. These parameters are listed in Table 3.1 and the simulation for each ranging algorithm will be run for 1000 different realizations of the channel model.

Table 3.1: Channel model parameter and simulation configuration

No	**Parameter**	**Value**
1	LOS Delay	20 ns
2	K - Factor	1
3	Ray interval rate (Λ)	0.25 [1/ns]
4	Ray decay constant (γ)	0.046 [dB/ns]
5	Signal to Noise Ratio (SNR)	20
6	Number of tones (K_f)	80
7	Hankel matrix ($\mathbf{H}$) dimension	41×40

3.2 Comparison between MF, MVDR, and MUSIC

As we may see in Figure 3.1, the MF algorithm creates the pseudospectrum as a sinc-like function. The main lobes occur at the estimated LOS delay. It is possible since the signals in this range of delays sum coherently, whereas it is not the case for other delay values. The number of sidelobes is equal to the number of rows in the matrix $\mathbf{H}$. The width of the main lobes is also related to the number of rows of $\mathbf{H}$. The width is around $1000/(L+1)$ ns. The width gets smaller for a higher number of L.

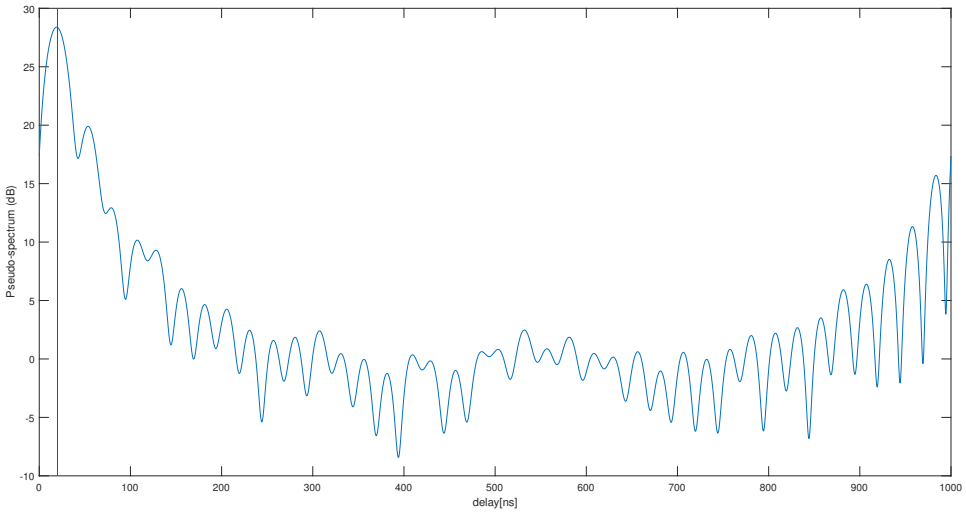

Figure 3.1: Matched Filter

In MVDR, the peak is generally sharper than in MF as illustrated in Figure 3.2. It shows that MVDR provides better resolution than MF.

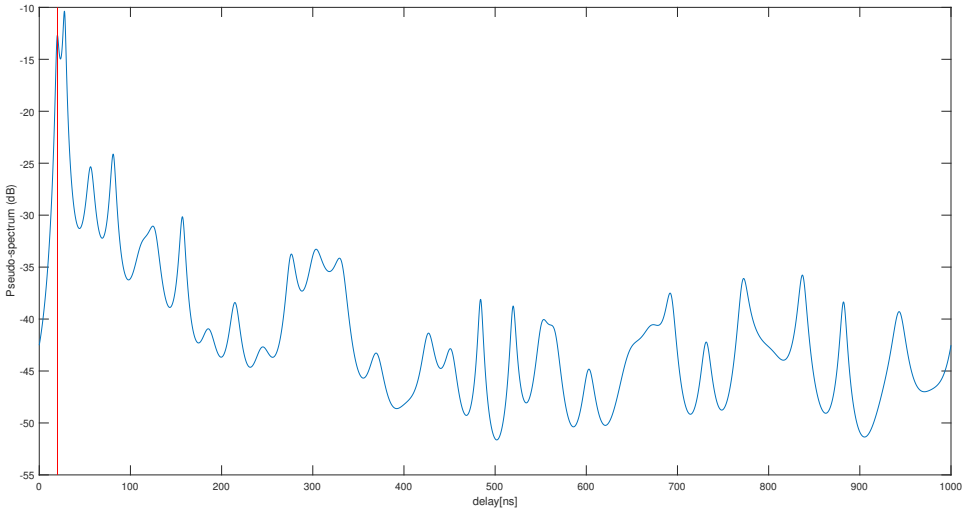

Figure 3.2: MVDR

Among all ranging algorithms, MUSIC provides the best resolution as shown in Figure 3.3. The width of the lobes is much shorter compared to MF, and the peak is slightly sharper than MVDR. In MUSIC, the first significant peak is located around 10-15 dB. The gap between the main lobes and most of the sidelobes is approximately

20 dB. Since we used $\mathbf{H}$ matrix of 41×40, it creates a $\overline{\mathbf{H}}$ with size 41×41, means we would assume the number of separable multipath is around half of the total number of columns of $\overline{\mathbf{H}}$, 20.

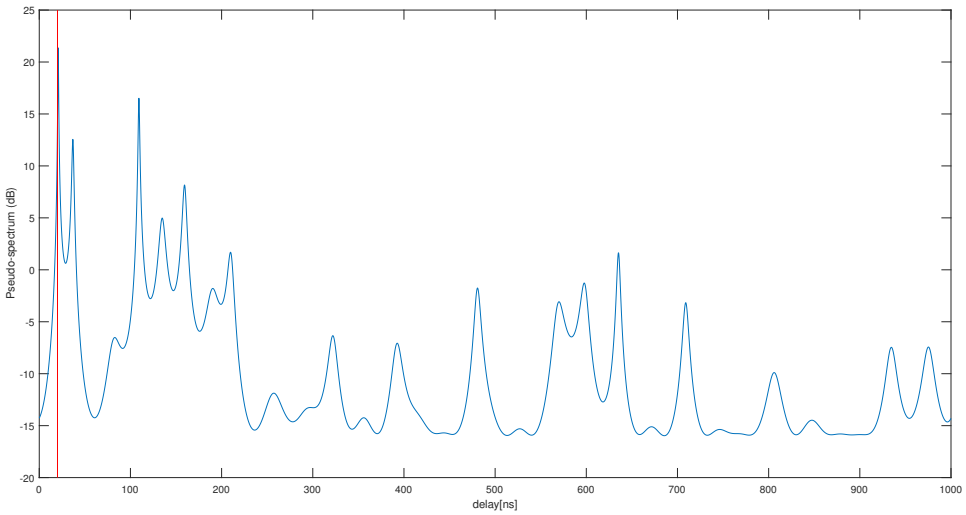

Figure 3.3: MUSIC

From Figure 3.4, MUSIC and MVDR give more robust results than MF. For the rest of this report, MUSIC is used over MVDR based on a better statistical performance as shown in Table B.1 in Appendix B.

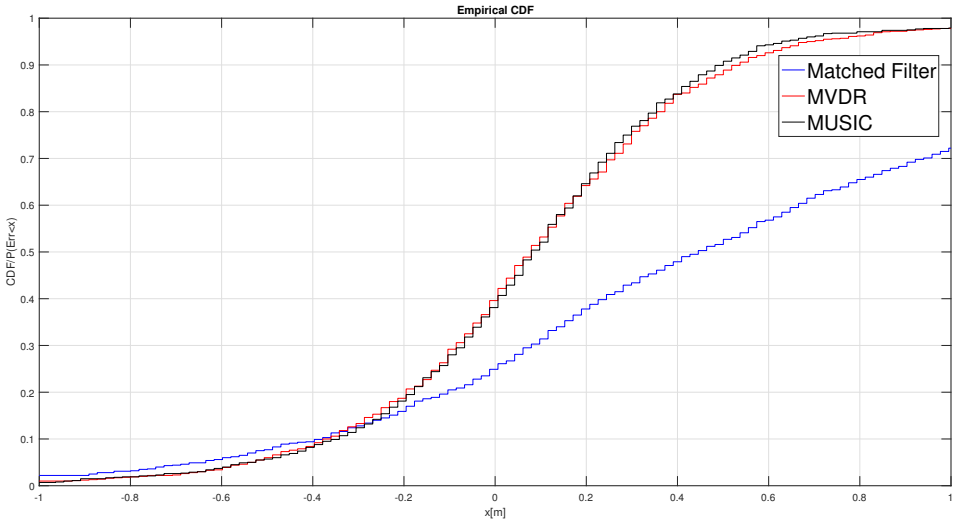

Figure 3.4: Cumulative Distribution Function (CDF) of Matched Filter, MVDR, and MUSIC

3.3 Comparison between square, wide, and tall matrix of H

As demonstrated in Figure A.1 and Figure A.2 in Appendix A the size of the **H** matrix plays a significant part on how the results of (pseudo)-spectrum looks. In Figure A.1, several high sidelobes are present, even though they can still be distinguished in comparison with the main lobe.

In Figure A.3, the (pseudo)-spectrum results for a wide matrix **H** is better than for the square matrix. Better results mainly due to a lower number of main lobes and higher orthogonality between the first main lobe and most of the sidelobes which are about 25 dB.

The pseudo-spectrum results in Figure A.2 show that a tall matrix performs the worst of all. It can be seen that it is unclear to determine the exact position of the first peak. High sidelobes also make a narrower gap to the primary lobe.

From Figure 3.5, there are ranging results based on 1000 different single-channel realizations with 20 dB of SNR(Signal to Noise Ratio). The results show that the MUSIC + Smoothing performance are quite similar regardless of the type of **H** matrix, regarding ranging bias. It shows that all of them have almost the same standard error. However, based on statistics result in Table B.2, the squared matrix of **H** will be chosen for the rest of this report since it still has small advantage result among others regarding median and standard deviation error.

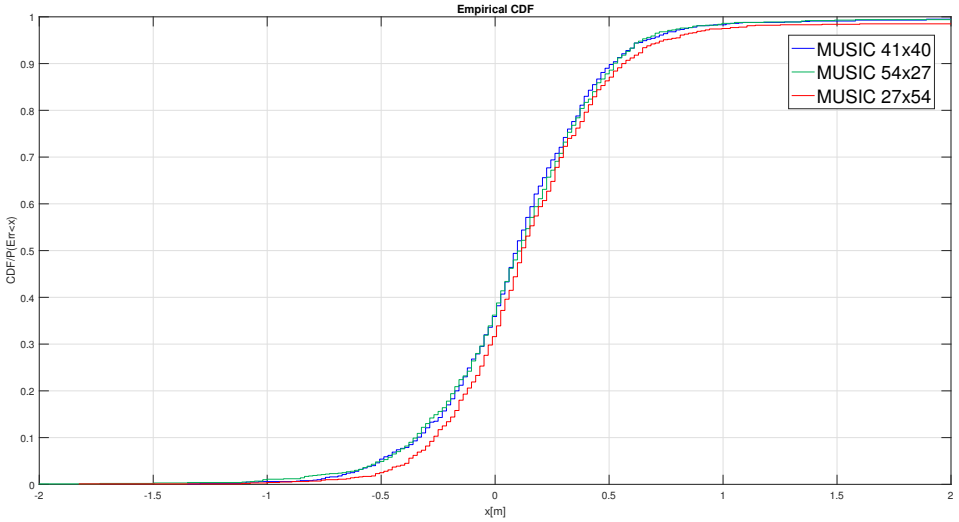

Figure 3.5: Cumulative Distribution Function (CDF) comparison of MUSIC + Smoothing results

3.4 MUSIC + Forward-Backward Smoothing

To increase the resolution of range estimation, a set of forward and conjugated backward subvectors are used, since it proves that to solve K correlated signals, it only needs $\frac{3}{2}K$

number of measurements, instead of $2K$. In this case, for $L+1$ number of subvectors, instead of just solving a maximum of $\lfloor \frac{L+1}{2} \rfloor$ different multipath components, now we can address a higher number $\lfloor \frac{2}{3}(L+1) \rfloor$. $\lfloor x \rfloor$ is $floor(x)$, the greatest integer number less than, or equal to x.

Instead of $\overline{\mathbf{H}}$, we now try to make the smoother type of matrix by forming a new square matrix $\overline{\mathbf{H}}_m$:

$$\overline{\mathbf{H}}_m \triangleq \mathbf{J}[\overline{\mathbf{H}}]^* \mathbf{J} \tag{3.1}$$

where * is the complex conjugate and $\mathbf{J}$ is the exchange matrix:

$$\mathbf{J} \triangleq \begin{pmatrix} 0 & 0 & \dots & 0 & 1 \\ 0 & 0 & \dots & 1 & 0 \\ \vdots & & \iddots & & \vdots \\ 0 & 1 & \dots & 0 & 0 \\ 1 & 0 & \dots & 0 & 0 \end{pmatrix} \tag{3.2}$$

Then, the new forward-backward smoothed covariance matrix is obtained by averaging between $\overline{\mathbf{H}}$ and $\overline{\mathbf{H}}_m$[28]:

$$\widetilde{\mathbf{H}} \triangleq \frac{1}{2(L+1)} (\overline{\mathbf{H}} + \overline{\mathbf{H}}_m) \tag{3.3}$$

Similar as in $\overline{\mathbf{H}}$ and $\overline{\mathbf{H}}_m$, $\widetilde{\mathbf{H}}$ also has a Hermitian matrix structure.

3.5 MUSIC + Forward-Backward Smoothing + AIC-MDL

Subspace methods like MUSIC could perform best with the exact information on the number of sources. However, in our case, this becomes a big problem since we do not know the number of separable multipath components. The first approach is then to look into the eigenvalues of the covariance matrix of $\overline{\mathbf{H}}$, before we discussed for the forward-backward covariance matrix of $\widetilde{\mathbf{H}}$ later in this section. Therefore, the Akaike Information Criterion (AIC) algorithm estimates the most likely number of sources within this condition, with the test is given by [29], [30], [31]:

$$AIC(N_s) = L_{N_s}(N_s) + p(N_s) \tag{3.4}$$

where $L_{N_s}(N_s)$ is a cost function based on Anderson's sufficient statistic in [32]:

$$L_{N_s}(N_s) = (K_f - L)(L - N_s + 1) \ln \left\{ \frac{\frac{1}{L-N_s+1} \sum_{i=N_s+1}^{L+1} \xi_i}{(\prod_{i=N_s+1}^{L+1} \xi_i)^{\frac{1}{L-N_s+1}}} \right\} \tag{3.5}$$

with ξ_i indicates the smallest $L - N_s$ eigenvalues of $\overline{\mathbf{H}}$, and $p(N_s)$ is a penalty term. The penalty term is indicated by the number of freely adjusted parameters in $\overline{\mathbf{H}}$ for conventional (or forward-only) smoothing, supposed there are N_s sources.

$\overline{\mathbf{H}}$ with N_s sources consists of $N_s + 1$ eigenvalues $(\xi_1, \dots, \xi_{N_s}, \sigma^2)$ and N_s eigenvectors$(\mathbf{u}_1, \dots, \mathbf{u}_{N_s})$, where $N_s \leq L + 1$. The eigenvalues are real and therefore count as $N_s + 1$ real parameters, while the eigenvectors are complex, unit norm,

and mutually orthogonal. It follows that $\overline{\mathbf{H}}$ has $2(L+1)$ parameters in each vector, and $2(L+1)N_s$ parameters for N_s vectors. However, not all of the parameters are free to vary. Each vector must have 1 element with a real number, means a reduction of N_s degrees of freedom (DOF). Furthermore, we have to deduct another N_s DOF due to their unit norm and $2(N_s(N_s-1)/2)$ due to their mutual orthogonalization since the eigenvectors follow certain constraints. Therefore, the total number of DOF is:

$$\begin{aligned} p(N_s) &= N_s + 1 + 2N_s(L+1) - N_s - N_s - N_s(N_s-1) \\ &= N_s(2(L+1) - N_s) + 1 \end{aligned} \tag{3.6}$$

The second term of the addition of one is an option that can be ignored, so:

$$p(N_s) \simeq N_s(2(L+1) - N_s) \tag{3.7}$$

and the AIC test is [33]:

$$AIC(N_s) \triangleq \{L_{N_s}(N_s) + [N_s(2(L+1) - N_s)]\}, \tag{3.8}$$

and

$$\hat{N}_{sAIC} = \underset{N_s}{\operatorname{argmin}}\{AIC(N_s)\}. \tag{3.9}$$

Based on this cost function, AIC can be defined as:

$$\hat{N}_{sAIC} = \underset{N_s}{\operatorname{argmin}}\{L_{N_s}(N_s) + N_s[2(L+1) - N_s])\} \tag{3.10}$$

Following Akaike's work, Schwartz [34] and Rissanen [31] made two different approaches. Schwartz [34] used the Bayesian approach, defining a prior probability to each model, and chose the model with maximum a posteriori probability. Rissanen's method is derived from an information theoretic argument. Rissanen suggested selecting the model that had the minimum code length since every model can be looked at as an encoding of the observation data. In the large-sample limit, both approaches gave the same criterion called Minimum Description Length (MDL):

$$\begin{aligned} MDL(N_s) &= L_{N_s}(N_s) + \frac{1}{2}p(N_s)\ln(K_f - L) \\ &= L_{N_s}(N_s) + \frac{1}{2}\Big[N_s[2(L+1) - N_s] + 1\Big]\ln(K_f - L) \end{aligned} \tag{3.11}$$

Note that the cost function of MDL is identical to AIC, while the penalty term has an extra factor of $\frac{1}{2}\ln(K_f - L)$, and

$$\hat{N}_{sMDL} = \underset{N_s}{\operatorname{argmin}}\{MDL(N_s)\}. \tag{3.12}$$

The MDL criterion is then given by:

$$\hat{N}_{sMDL} = \underset{N_s}{\operatorname{argmin}}\left\{L_{N_s}(N_s) + \frac{1}{2}\Big[N_s[2(L+1) - N_s] + 1\Big]\ln(K_f - L)\right\} \tag{3.13}$$

As discussed in the previous sub-chapter, forward-backward approach gives benefit in averaging a coherent or correlated signal environment. Therefore, the detection tests now must be adjusted to account for the use of $\widetilde{\mathbf{H}}$ instead of $\overline{\mathbf{H}}$.

If forward-backward smoothing applies, the AIC formulation change since FB averaging alter the Hermitian structure of $\overline{\mathbf{H}}$ into both Hermitian and centro-Hermitian property in $\widetilde{\mathbf{H}}$, or in other words:

$$\widetilde{\mathbf{H}} = \mathbf{J}[\widetilde{\mathbf{H}}]^*\mathbf{J} \tag{3.14}$$

In the FB case, the eigenvectors $\{\mathbf{u}_i\}$ corresponding to different eigenvalues can be chosen as centro-Hermitian vectors, which has a property $\mathbf{u}_i = \mathbf{J}\mathbf{u}_i^*$. It means that the bottom half elements of the vector are only conjugates of the top half elements resulting in free parameters for half of the total elements. Assume that $(L+1)$ is even, then there are only $\frac{1}{2}2(L+1)$ free parameters in each centro-Hermitian vector, or $N_s(L+1)$ free parameters in N_s number of sources.

$\widetilde{\mathbf{H}}$ with N_s sources still consists of N_s largest eigenvalues, $(L+1)-N_s$ repeated eigenvalues of σ^2, and N_s eigenvectors. However, centro-Hermitian properties as explained above reduce DOF for $\frac{1}{2}2(L+1)$. Then, the constraints of unit norm and mutual orthonormality reduces DOF by N_s and $\frac{1}{2}N_s(N_s-1)$.

The penalty term is now changed due to the introduction of FB averaging [35]:

$$\begin{aligned} p(N_s) &= N_s + 1 + 2N_s(L+1) - N_s(L+1) - N_s - \frac{N_s(N_s-1)}{2} \\ &= \frac{1}{2}N_s(2(L+1) - N_s + 1) + 1 \end{aligned} \tag{3.15}$$

or neglecting the constant of one,

$$p(N_s) \simeq \frac{1}{2}N_s(2L - N_s + 3) \tag{3.16}$$

The AIC-FB and MDL-FB functions are:

$$\begin{aligned} \hat{N}_{sAIC:FB} &= \underset{N_s}{\operatorname{argmin}}\{L_{N_s}(N_s) + \frac{1}{2}N_s[2(L+1) - N_s + 1]\} \\ &= \underset{N_s}{\operatorname{argmin}}\{L_{N_s}(N_s) + \frac{1}{2}N_s(2L - N_s + 3)\} \end{aligned} \tag{3.17}$$

and

$$\begin{aligned} \hat{N}_{sMDL:FB} &= \underset{N_s}{\operatorname{argmin}}\{L_{N_s}(N_s) + \frac{1}{4}N_s[2(L+1) - N_s + 1]\ln(K_f - L)\} \\ &= \underset{N_s}{\operatorname{argmin}}\{L_{N_s}(N_s) + \frac{1}{4}N_s(2L - N_s + 3)\ln(K_f - L)\} \end{aligned} \tag{3.18}$$

where the $L_d(N_s)$ is given by (3.5), with the ξ_i is the eigenvalues of $\widetilde{\mathbf{H}}$ now.

We can see that FB averaging is reducing the free adjustable parameters by a factor of 2. The tests still have similar structure since the only change is in the penalty

function. After that, we find the value of N_s that minimize (3.17) and (3.18) and expressed it by $\hat{N}_s$.

In [29], it shows that both MDL and MDL-FB are consistent. It means that as K_f goes to infinity, $\hat{N}_{sMDL}$ and $\hat{N}_{sMDL:FB}$ approach N_s. On the other hand, AIC is inconsistent and, asymptotically, tends to overestimate the number of signals. Nevertheless, for a small K_f the AIC generally has a better probability of a right decision. Therefore, based on this information, the number of signals $\hat{N}_s$ in this simulation are then decided as the minimal value among $\hat{N}_{sAIC:FB}$ and $\hat{N}_{sMDL:FB}$.

3.6 Results

3.6.1 MUSIC + Forward-Backward Smoothing

In Figure 3.6, we see the effect of forward-backward smoothing where the first main lobes are located around 30 to 35 dB. It is approximately 20 dB higher in comparison with forward-only smoothing, given the similar power of the sidelobes. From the Table B.3 in Appendix B, FBS clearly reduces the standard deviation error about 20%.

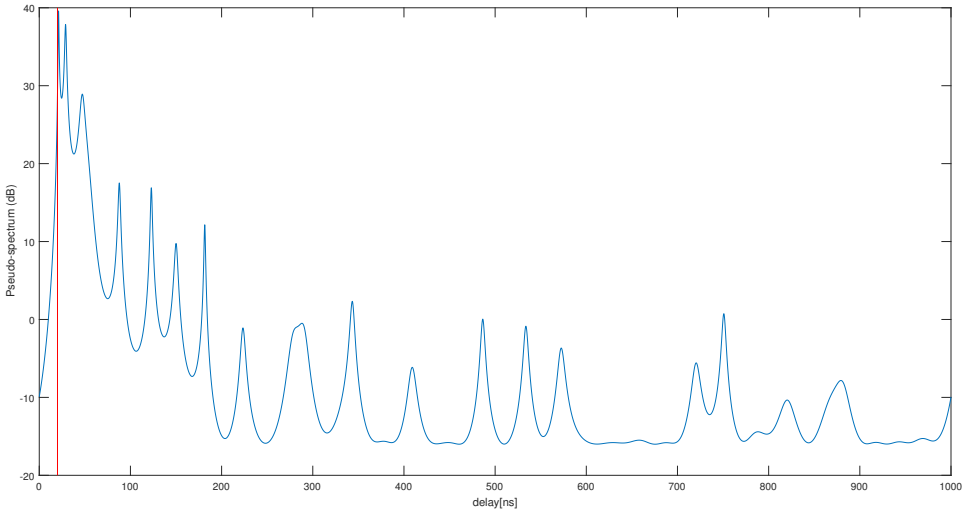

Figure 3.6: An example of the pseudo-spectrum of MUSIC + Forward Backward Smoothing with **H** size of 41×40

3.6.2 MUSIC + Forward-Backward Smoothing + AIC-MDL

In Figure 3.7, the effect of inserting AIC - MDL is seen by diminishing most of the sidelobes. It also results in the higher energy at the rest of the lobes since the number of sources are now significantly reduced. It can also be seen that the number of sources N_s for a squared **H** matrix now estimated at around 6, instead of just halves total number of rows, 20.

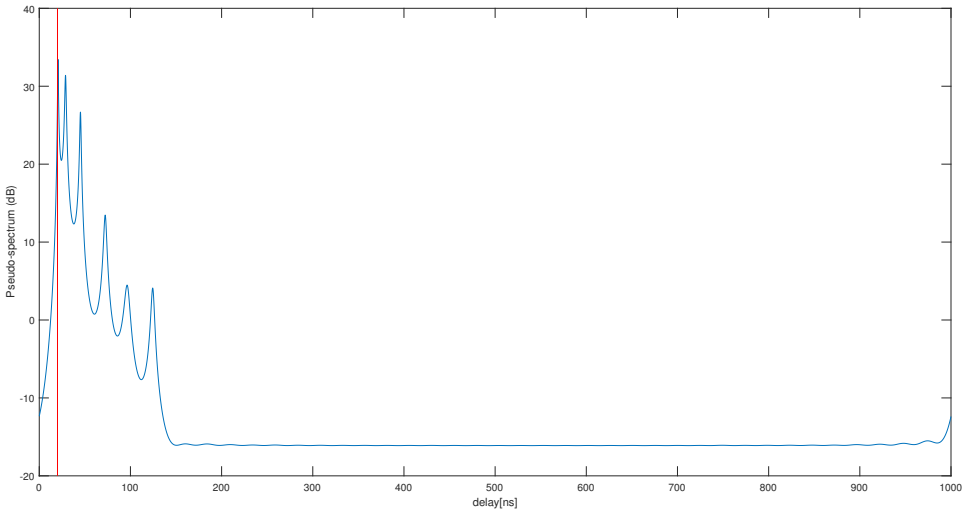

Figure 3.7: An example of the pseudo-spectrum of MUSIC + Forward Backward Smoothing + AIC - MDL with $\mathbf{H}$ size of 41×40

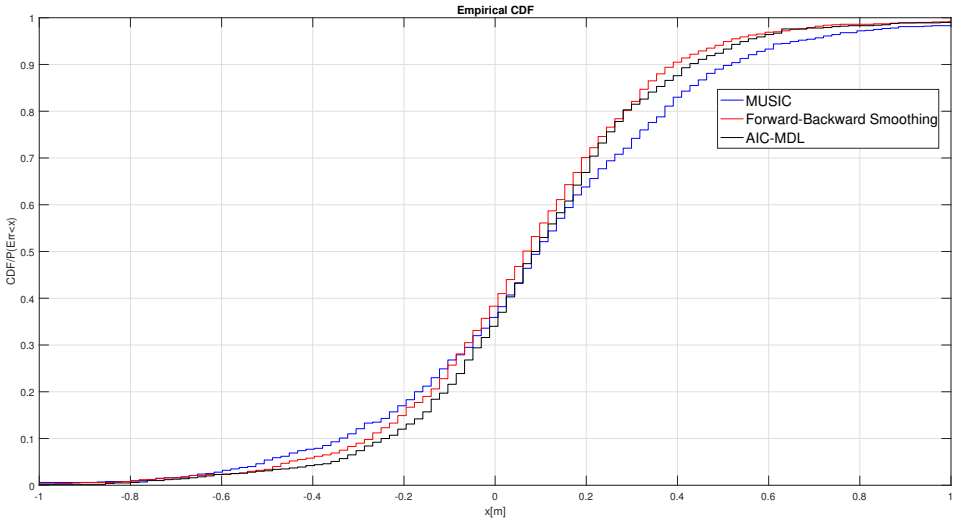

Figure 3.8: CDF Comparison of MUSIC + Forward-Backward Smoothing + AIC MDL Results, K-factor $= 1$, $\Lambda = 0.25$ [1/ns]

From Table B.4 and Figure 3.8, it can be seen that there is some additional ranging performance result of MUSIC by inserting AIC-MDL. In fact, the best ranging result is shown on a squared matrix case.

Insertion of AIC-MDL undoubtedly reduce the outliers and standard deviation of

ranging bias. It is shown that the standard deviation of AIC-MDL is now 0.344 m, compared to forward-backward smoothing and MUSIC with 0.402 m and 0.491 m, respectively. An improvement in minimizing standard deviation probably because AIC-MDL reduces all sidelobes which do not belong to expected sources. Therefore the range probability of peak detection is now much narrower than in MUSIC.

3.7 Bias Compensation for MUSIC + Forward-Backward Smoothing + AIC-MDL

Figure 3.9 and Table C.1 compare the results of the ranging algorithms in Figure 3.8 and its bias compensation. Bias compensation is done by computing another different set of data for calculating the bias and subtracting it with the bias from the previous data set. Overall, the empirical CDF shows a reduction of bias for FBS and AIC-MDL. It is shown that the median bias is around 0 m after compensation. Median is the statistics chosen instead of mean as it is less affected by the effect of outliers.

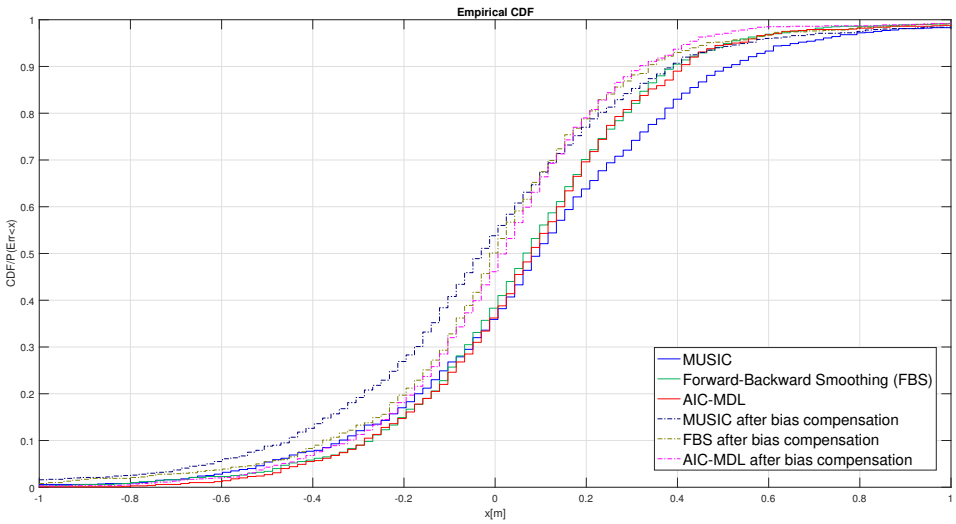

Figure 3.9: CDF comparison of MUSIC + Forward-Backward Smoothing + AIC MDL Results, K-factor = 1, $\Lambda = 0.25$ [1/ns], before and after bias compensation

3.8 Conclusion

In this chapter, we proposed more advanced ranging algorithms which tackle the multipath effect as the main problem in the previous chapter. In the first part of this chapter, we compared and evaluated the performance of Matched Filter, MVDR, and MUSIC. The results showed that MUSIC provided a better performance over MF and MVDR. Also, MUSIC performs better in a structure of square matrix of $\mathbf{H}$ than in wide or tall structure. In the second part of this chapter, Forward-Backward Smoothing and AIC-MDL are introduced and applied on top of MUSIC algorithm to reduce further the standard deviation in ranging results by diminishing the multipath effect and estimating the number of separable multipath in the channel.

4 Bias Compensation

Previously, the addition of FBS and AIC-MDL has been able to reduce the outliers of the ranging estimation as discussed in Chapter 3. However, both of them are still unable to overcome the bias as in the MUSIC algorithm. In this chapter, we proposed a bias compensation in order to try to remove the bias. The impact of bias compensation is then examined through different channel model parameter combinations.

4.1 Procedure of compensating bias in ranging

The diagram in Figure 4.1 proposes the process of bias compensation in real ranging. The process could be done by exploiting the benefit of the simulation of bias compensation.

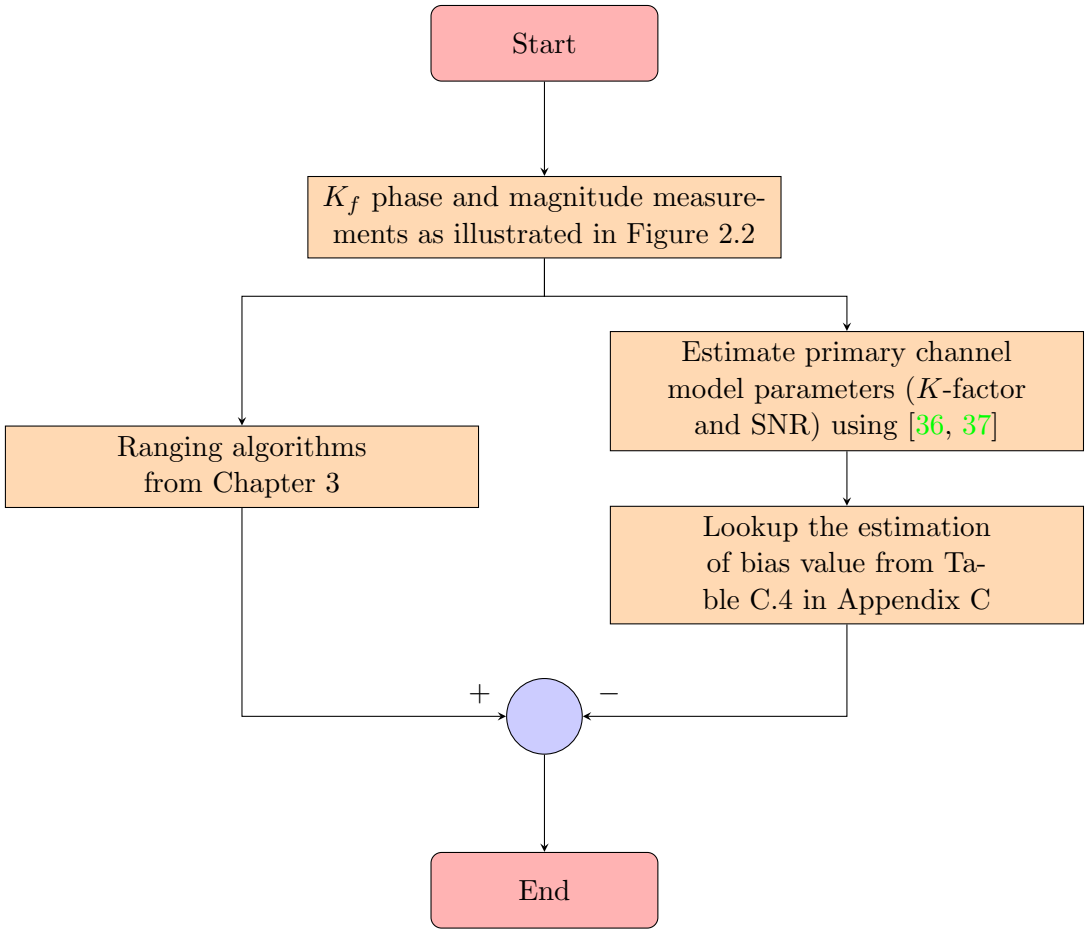

Figure 4.1: Block diagram of compensating bias in ranging

At the first stage in the process, the K_f tones are measured as explained in Figure 2.2. The result of the phase difference can be split into two different parallel steps. One of them is to reduce the effect of multipath by using the proposed ranging algorithms from Chapter 3. The other step is estimating the main channel model parameters.

Throughout this chapter, we may study that K-factor and SNR are chosen as the primary characteristics of the model which contribute significantly to the bias value since it may be difficult to estimate all possible model parameters. Ramesh et al. in [36] estimate K-factor using a statistical ratio of observables over a block of data in a generalized fading channel, while Abdi et al. [37] estimate SNR using higher-order statistics. Results of the K-factor and SNR estimation will be the base of the lookup table to estimate the value of bias further as shown in Table C.4 in Appendix C.

In the last step, the result of bias estimation subtracts the result of the ranging algorithm to get the final results of ranging.

4.2 Ranging bias for different K-factor and Λ

Figure 4.2 and Table C.2 illustrates the estimated ranging bias for varying parameter values of K-factor and Λ. The value of K-factor differs from 0.1 to 1, with an increment of 0.1, while the value of Λ differs from 0.1 ns to 1 ns, with an increment of 0.1. Overall, both K-factor and Λ tend to impact the bias value of the range estimation. Lower K-factor means a higher proportion of NLOS signals compared to the LOS signals. It leads to a higher estimation bias. A similar situation also happens for a higher Λ since it increases the arrival rate of each multipath component.

The figure shows that K-factor has a more significant impact on ranging bias than Λ. The gradient of the curve explains this situation. However, there is a considerable drop in bias value from 0.1 to 0.2 in the ray interval rate. This drop is possible since for Λ equal to 0.2, the gap between each ray is around 5 ns. Meanwhile, the gap becomes approximately 10 ns for Λ equal to 0.1, which is sparse already. Implicitly, we may see that the resolution for AIC-MDL is between 5 ns and 10 ns in this case.

4.3 Ranging bias for different K-factor and Λ after bias compensation

The mesh plot in Figure 4.3 displays the impact of bias correction of the results from Section 4.2 and Table C.3 in Appendix C. Overall, the ranging bias now reduced to an absolute value below 0.08 m for all combinations of both K-factor and Λ, as also shown in Table C.3. The bias value now just fluctuated slightly from -0.034 m until up to 0.073 m, compared with 0.043 m to 0.62 m previously without bias compensation.

As the bias correction is now added into the ranging results, the bias for all ranging results for different values of K-factor and Λ is more or less similar. These results show that the proposed approach could refine the ranging results for all parameter values of K-factor and Λ.

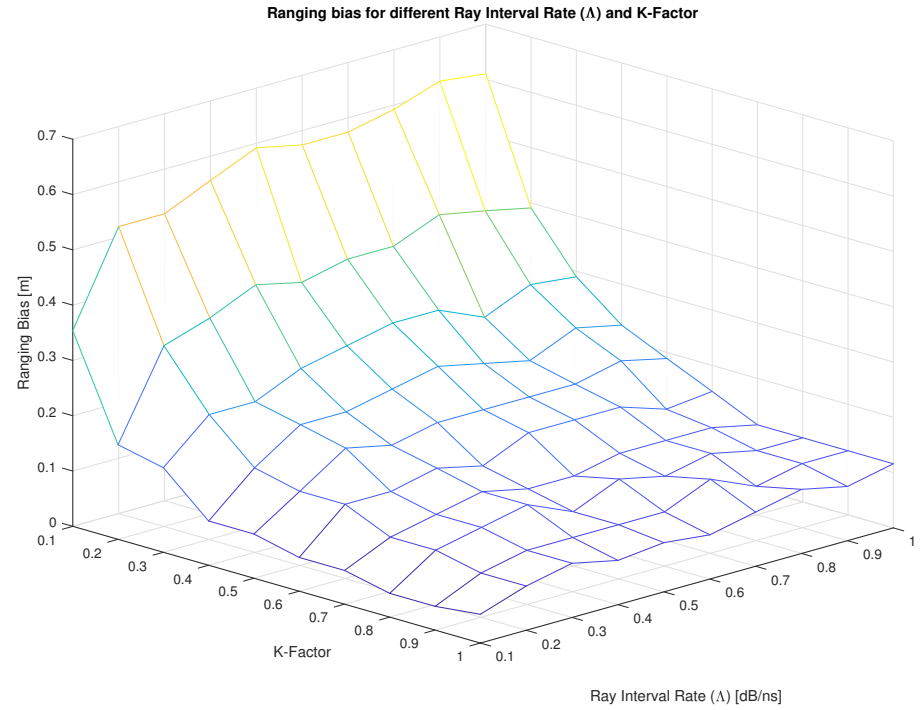

Figure 4.2: Mesh plot of ranging bias for different K-factor and Λ

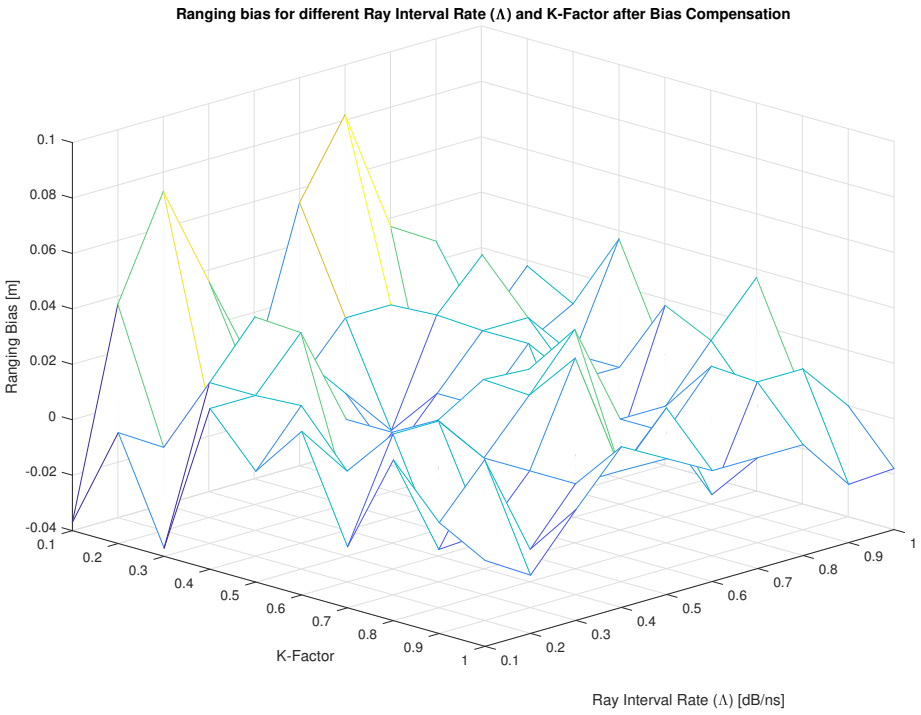

Figure 4.3: Mesh plot of ranging bias for different K-factor and Λ after bias compensation

4.4 Ranging bias for different SNR and K-factor

Figure 4.4 and Table C.4 provides ranging bias results for different values of K-factor and another parameter, SNR. It is clear that ranging results change significantly for various values of K-factor and SNR.

In contrary to the effect of Λ in Section 4.2, SNR is a more influential parameter in estimating the bias value. It is shown that increasing the SNR value up to around 9 dB could affect reducing the bias to less than half. For example, for K-factor equal to 0.6, the ranging bias can differ from 0.263 m with 11 dB of SNR to 0.134 m with 20 dB of SNR. A similar pattern is also shown for other values of the K-factor. Based on these facts, it is shown that the worst ranging bias is 0.904 m for 0.1 of K-factor and 11 dB of SNR, whereas the best ranging bias is 0.08 m for K-factor equal to 1 and 20 dB of SNR, showing around 0.9 m of bias difference.

Both the mesh plot and the table only show the results varying the SNR from 20 dB to as little as 11 dB, because, for an SNR lower than 11 dB together with a low K-factor, the interested peak becomes very weak and indistinguishable from the sidelobes.

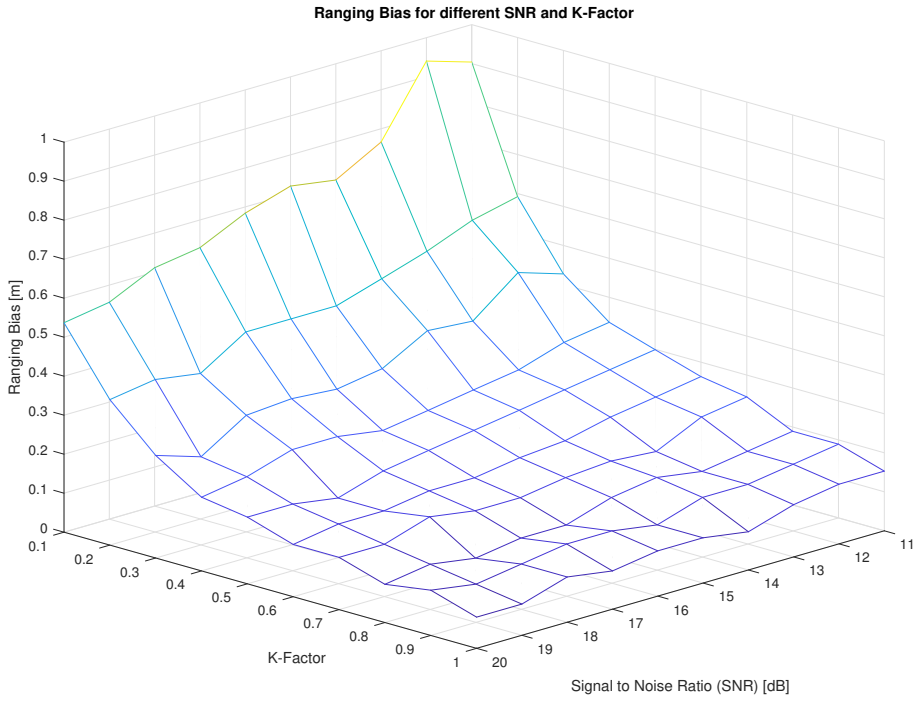

Figure 4.4: Mesh plot of ranging bias for different SNR and K-factor

4.5 Ranging bias for different SNR and K-factor after bias compensation

Figure 4.5 and Table C.5 illustrate the impact of bias compensation for all combinations of SNR and K-factor based on the results in Section 4.4. The results are shown as ranging bias in meter unit.

Overall, the proposed correction reduces the absolute bias value up to below 0.08 m for all different parameter values of SNR and K-factor. The bias value now only differs from -0.073 m to 0.055 m, where some of them show a perfect bias value of 0 m.

As the bias compensation is now added to the result of ranging bias, the bias values of K-factor and SNR are more or less similar. It proves that the proposed approach could also improve the ranging result for all parameter values of K-factor and SNR.

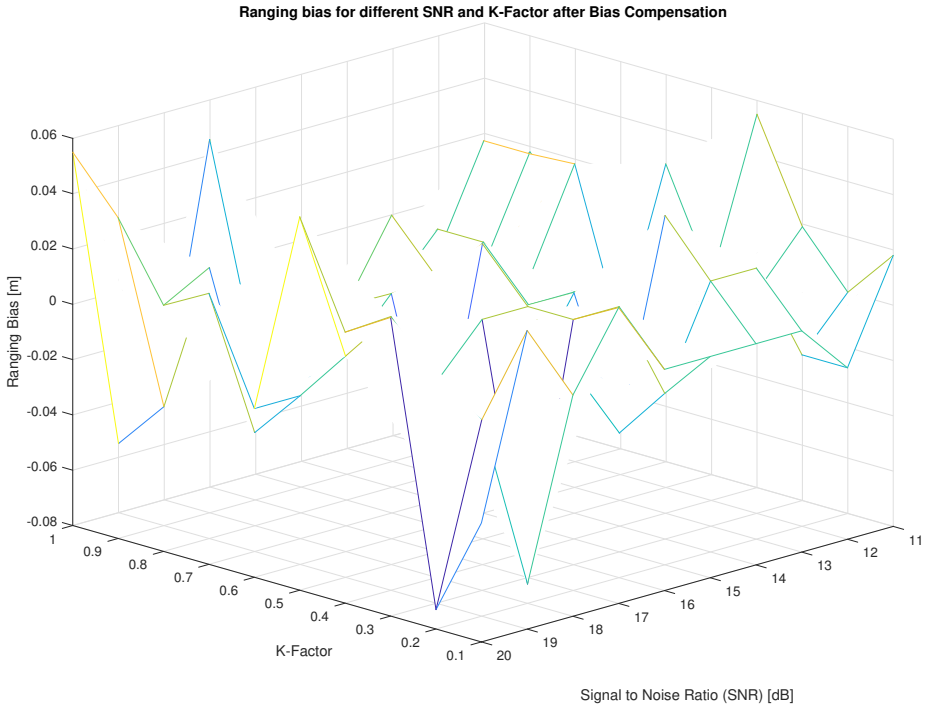

Figure 4.5: Mesh plot of ranging bias for different SNR and K-factor after bias compensation

4.6 Ranging bias for different K-factor and γ

Figure 4.6 and Table C.6 in Appendix C show the ranging bias with value variation in two different parameters of K-factor and γ. The results are shown in the meter unit. Overall, it is quite evident that γ has almost no influence on the ranging bias. It is probably due to a common low value of γ set in the channel parameter. The value of parameter γ varies from 0.01 to 0.1 dB/ns.

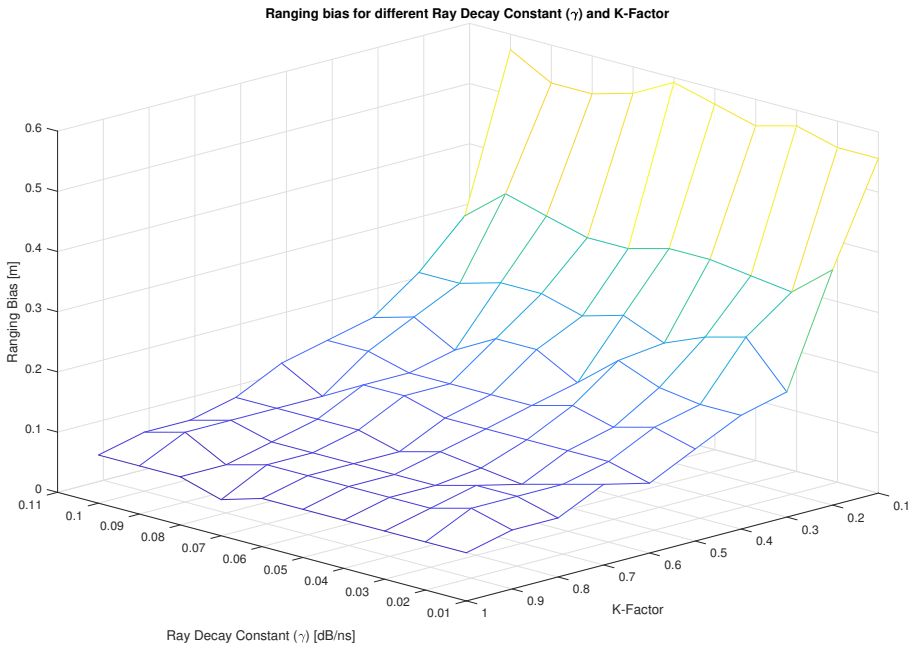

Figure 4.6: Mesh plot of ranging bias for different K-factor and γ

It is clear from both the mesh plot and the table that changing the γ value for all conditions of K-factor, has little impact on the ranging result. For instance, for a K-factor equal to 0.5, the ranging bias only changes from 0.153 m for 0.01 dB/ns of γ to 0.171 m for 0.1 dB/ns of γ. There is only around 0.02 m difference in bias.

4.7 Ranging bias for different K-factor and γ after bias compensation

Figure 4.7 and Table C.7 provide a ranging result of bias compensation for different values of K-factor and γ from Section 4.6.

It can be seen from the mesh plot that the ranging bias is stagnated for all different values of K-factor and γ. The bias value now only varies from -0.074 m to 0.038 m, where some of them also show perfect bias value of 0 m.

To conclude, bias compensation is able to refine the ranging results for all parameter values of K-factor and γ.

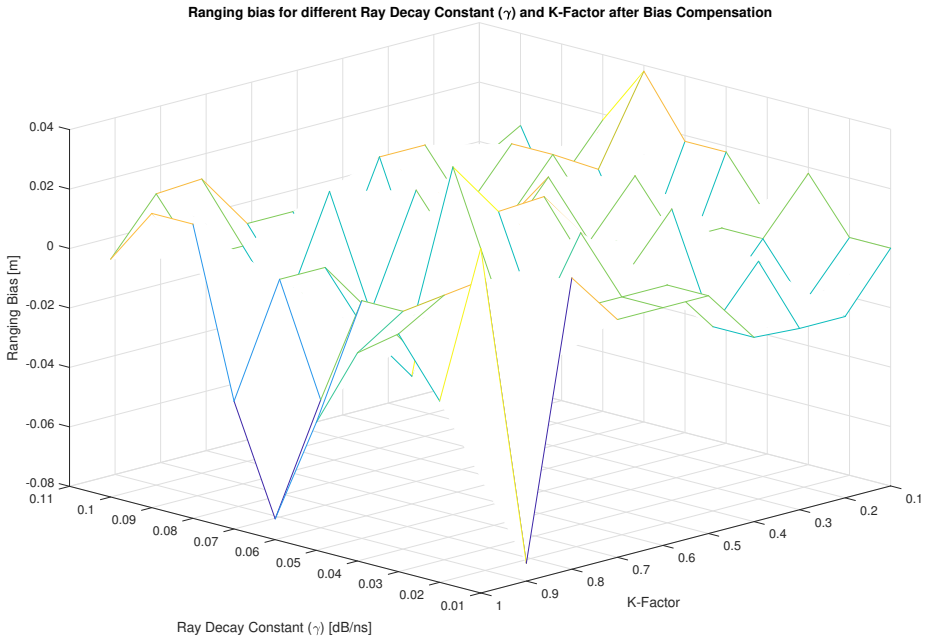

Figure 4.7: Mesh plot of ranging bias for different K-factor and γ after bias compensation

4.8 Conclusion

In this chapter, we proposed a method to reduce further the bias in ranging. In the first part of the chapter, we illustrated the flowchart of compensating ranging bias in real life. In the later part of the chapter, we investigated the effect of several essential channel parameters, such as K-factor, ray interval rate (Λ), and SNR. Results of different combinations of the parameters are shown in a mesh plot and raw data table in the appendix. The performance advantage of compensating this bias is also shown in this chapter.

5 MUSIC-Like

In this chapter, a variation of ranging algorithm is presented by introducing a different optimization problem. The goal of this optimization problem is minimizing the variance of the output array subject to keep the output power at each delay and avoid a trivial solution. The problem is called as a MUSIC-Like method, having similarities with MUSIC in some special cases, but not based on subspace methods and not estimating the number of separable multipath.

5.1 Overview

Previously, MF and MVDR is applied as a ranging estimation technique to solve the problem. Both MF and MVDR do not need any information about source number. However, it can be seen from Chapter 3 that MF and MVDR could not provide a resolution as high as MUSIC. However, MUSIC is a technique that demands subspace decomposition to determine the constraint which already estimated by AIC-MDL.

The results in Chapter 4 show that SNR is a vital channel parameter since the ranging performance deteriorates by around half for a 9 dB difference. Djurić [38] also indicates that AIC and MDL are prone to estimating a wrong number of sources for low SNR and a small number of samples in DOA problem. An error in determining the model order of the signal subspace could affect the overall performance of the subspace-based methods like MUSIC. Therefore, a declining ranging performance due to a false approximation of separable multipath numbers should be prevented.

In this chapter, a new optimization problem is proposed which not based on the subspace decomposition hence it does not need the number of sources. Instead, the solution of this optimization problem will look at the eigenvector associated with the smallest eigenvalue of the matrix which relies on both the delay and the smoothed covariance matrix, $\overline{\mathbf{H}}$. The algorithm is called as MUSIC-like [39].

The MUSIC-like algorithm does not need a split between signal and noise subspaces. In [39], the algorithm is addressed as MUSIC-like even though this technique does not depend on the subspace decomposition since it follows the MUSIC algorithm in two aspects: the equivalent spectral spectrum in the absent of sources for DOA case and optimal weight vector specified by the weighted sum of noise eigenvectors. This algorithm claimed to perform better than MUSIC with AIC-MDL under low SNR conditions [40].

5.2 Problem Statement

The proposed algorithm solves the optimization problem given as:

$$\begin{aligned} \min_{\mathbf{w}} \quad & \mathbf{w}^{\mathrm{H}}\overline{\mathbf{H}}\mathbf{w} \\ \text{subject to} \quad & \mathbf{w}^{\mathrm{H}}\mathbf{e}(\tau)\mathbf{e}(\tau)^{\mathrm{H}}\mathbf{w} + \beta \parallel \mathbf{w} \parallel_2^2 = \mathbf{w}^{\mathrm{H}}\{\mathbf{e}(\tau)\mathbf{e}(\tau)^{\mathrm{H}} + \beta\mathbf{I}_{L+1}\}\mathbf{w} = c \end{aligned} \tag{5.1}$$

where $c, \beta > 0$ are constants. The constraint in (5.1) is different than MVDR in (2.23) as using output power rather than the output signal copy itself. Therefore, this algorithm is proposed constraint on the power gain at delay τ with L_2 norm constraint of the weight vector [41].

The following Lagrangian function can be constructed using the Lagrange multiplier technique:

$$L(\mathbf{w}, \lambda) = \mathbf{w}^{\mathrm{H}}\overline{\mathbf{H}}\mathbf{w} - \lambda\Big(\mathbf{w}^{\mathrm{H}}\Big\{\mathbf{e}(\tau)\mathbf{e}(\tau)^{\mathrm{H}} + \beta\mathbf{I}_{L+1}\Big\}\mathbf{w} - c\Big) \tag{5.2}$$

where λ is the Lagrangian multiplier. Setting the gradient of $L(\mathbf{w}, \lambda)$ with respect to the weight vector $\mathbf{w}$ to zero gives:

$$\overline{\mathbf{H}}\mathbf{w} = \lambda\Big(\mathbf{e}(\tau)\mathbf{e}(\tau)^{\mathrm{H}} + \beta\mathbf{I}_{L+1}\Big)\mathbf{w} \tag{5.3}$$

It can be seen that the formulation becomes a generalized eigenvalue problem, with the pair of $\big\{\overline{\mathbf{H}}, (\mathbf{e}(\tau)\mathbf{e}(\tau)^{\mathrm{H}} + \beta\mathbf{I}_{L+1})\big\}$ is called as matrix pencil [42, 43]. Since $\big(\mathbf{e}(\tau)\mathbf{e}(\tau)^{\mathrm{H}} + \beta\mathbf{I}_{L+1}\big)$ is an invertible matrix, then λ is the generalize eigenvalue of $\big(\mathbf{e}(\tau)\mathbf{e}(\tau)^{\mathrm{H}} + \beta\mathbf{I}_{L+1}\big)^{-1}\overline{\mathbf{H}}$. Multiplying both sides from (5.3) on the left with $\mathbf{w}^{\mathrm{H}}$ yields:

$$\mathbf{w}^{\mathrm{H}}\overline{\mathbf{H}}\mathbf{w} = \lambda\mathbf{w}^{\mathrm{H}}\{\mathbf{e}(\tau)\mathbf{e}(\tau)^{\mathrm{H}} + \beta\mathbf{I}_{L+1}\}\mathbf{w} = \lambda c \tag{5.4}$$

is the one that we want to minimize looking back at (5.1). Therefore, the optimal weight vector is the eigenvector associated with the minimum eigenvalue of $\big(\mathbf{e}(\tau)\mathbf{e}(\tau)^{\mathrm{H}} + \beta\mathbf{I}_{L+1}\big)^{-1}\overline{\mathbf{H}}$. It also can be seen just the selection of β that influence the optimal weight vector, while the value of c is not crucial for this algorithm. The value of c will only be totally adjusted by the optimization problem.

Given the Sherman-Morrison formula [44, 45]:

$$(\mathbf{A} + \mathbf{b}\mathbf{c}^{\mathrm{H}})^{-1} = \mathbf{A}^{-1} - \frac{\mathbf{A}^{-1}\mathbf{b}\mathbf{c}^{\mathrm{H}}\mathbf{A}^{-1}}{1 + \mathbf{c}^{\mathrm{H}}\mathbf{A}^{-1}\mathbf{b}} \tag{5.5}$$

the inverse of $\big(\beta\mathbf{I}_{L+1} + \mathbf{e}(\tau)\mathbf{e}(\tau)^{\mathrm{H}}\big)^{-1}$ is equal to:

$$\begin{aligned} (\beta\mathbf{I}_{L+1} + \mathbf{e}(\tau)\mathbf{e}(\tau)^{\mathrm{H}})^{-1} &= \beta^{-1}\mathbf{I}_{L+1} - \frac{\beta^{-2}\mathbf{e}(\tau)\mathbf{e}(\tau)^{\mathrm{H}}}{1 + \beta^{-1}\mathbf{e}(\tau)^{\mathrm{H}}\mathbf{e}(\tau)} \\ &= \beta^{-1}\mathbf{I}_{L+1} - \frac{\beta^{-2}\mathbf{e}(\tau)\mathbf{e}(\tau)^{\mathrm{H}}}{1 + \beta^{-1}(L+1)} \end{aligned} \tag{5.6}$$

A suggested choice for β is derived in [40] as:

$$\beta = (1-\alpha)\beta_{\min} + \alpha\beta_{\max} \tag{5.7}$$

where $0 < \alpha < 1$. The value of α is given by:

$$\alpha = \frac{\beta_{\min}}{\beta_{\max}} = \frac{\max\limits_{\hat{\tau}} \mathbf{e}(\tau)^{\mathrm{H}} \overline{\mathbf{H}}^{-1} \mathbf{e}(\tau)}{\min\limits_{\hat{\tau}} \mathbf{e}(\tau)^{\mathrm{H}} \overline{\mathbf{H}}^{-1} \mathbf{e}(\tau)} \tag{5.8}$$

where both $\beta_{\min}$ and $\beta_{\max}$ are equivalent to the peak and floor of the MVDR output power, respectively.

Given the optimal weight vector $\mathbf{w}$, the spectrum LOS delay is then estimated by finding the first peak of $\hat{P}_{MU-Like}(\tau)$:

$$\hat{P}_{MU-Like}(\tau) = \frac{1}{\left|\mathbf{w}^{\mathrm{H}} \mathbf{e}(\tau)\right|^2} \tag{5.9}$$

which is different from the power response derived by MVDR estimator.

The implementation of the MUSIC-Like algorithm can be summarized using the following steps:

1. Select a suitable β based on (5.7)
2. Calculate $\widetilde{\mathbf{B}} = \left(\beta \mathbf{I}_{L+1} + \mathbf{e}(\tau)\mathbf{e}(\tau)^{\mathrm{H}}\right)^{-1} \overline{\mathbf{H}}$ as shown in (5.6)
3. Find the eigenvector with respect to the minimum eigenvalue of $\widetilde{\mathbf{B}}$
4. Calculate the spectrum according to (5.9)

5.3 Simulation Results

Figure 5.1 shows the (pseudo)-spectrum of MUSIC-like. It is observed that MUSIC-like has a similar spectrum and resolution with MUSIC in Figure 3.3. The first peak located at the estimated LOS delay. It shows that MUSIC-like is capable as a ranging algorithm for this channel model. Table B.1 in Appendix B presents the statistical performance of MUSIC-like among previous ranging algorithm using the same channel parameter in Table 3.1. It can be seen that the performance of MUSIC-like is similar to AIC-MDL under high SNR conditions.

The advantage of the MUSIC-like algorithm over AIC-MDL can be seen under low SNR environments. In low SNR conditions, a model order estimation techniques like AIC-MDL are unable to assure correct results. Figure 5.2 depicts the ranging performance of MUSIC-like compare with MUSIC decoupled with AIC-MDL. Ranging bias equal to zero is also plotted for reference. MUSIC-like and AIC-MDL have only marginal difference performance under high SNR (above 0 dB). However, AIC-MDL is started to unable to perform satisfactorily for SNR below -7 dB. In such conditions, MUSIC-like has a better capability to estimate the LOS delay.

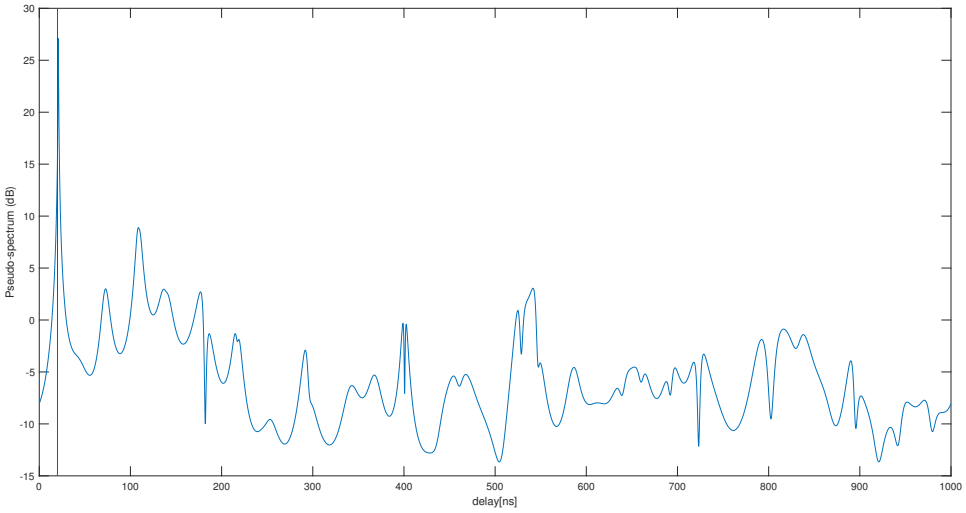

Figure 5.1: MUSIC-Like

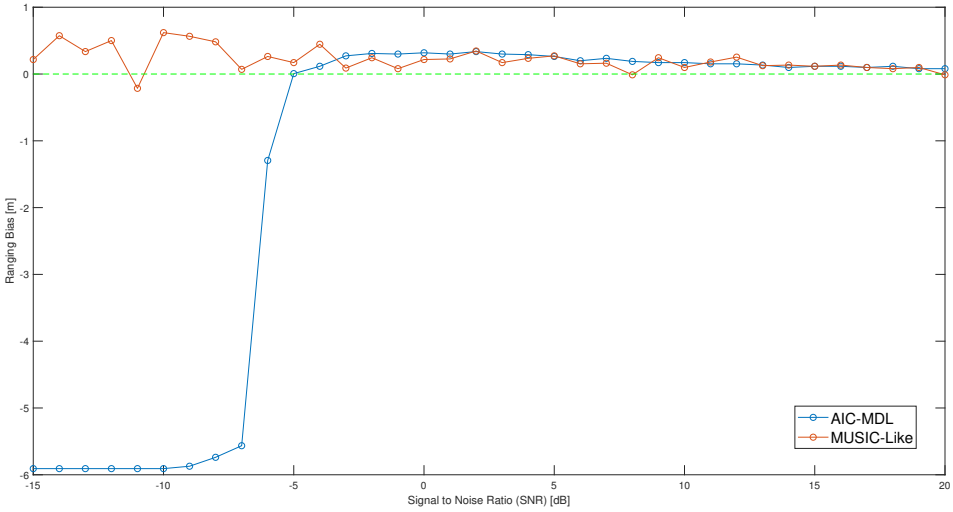

Figure 5.2: Performance comparison between MUSIC-Like and AIC-MDL

5.4 Conclusion

In this chapter, MUSIC-like is an algorithm presented without estimating the number of sources. It can be seen that MUSIC-Like has two advantages compares to the previous methods. First, this algorithm does not require the information about the number of sources to estimate the LOS delay. Second, the performance of MUSIC-like still gives better performance compare to MUSIC coupled with AIC-MDL algorithm under adverse SNR conditions.

6 Concluding Remarks

6.1 Conclusions

The major objective of this thesis is to improve the ranging accuracy in the narrow-band indoor environments using industrial, scientific, and medical (ISM) radio bands exploiting various signal processing approaches. Previously, the phase difference method was proposed. Phase difference is a compatible technique for a single-ray pure line of sight (LOS) channel model. However, the phase difference method is not entirely suitable for the multi-ray radio channel model. In this channel model, both LOS and non-line of sight (NLOS) paths are present. For this reason, a combination with a direction of arrival (DOA) algorithm is needed with the aim of minimizing the ranging bias. In Chapter 3, the performance of various DOA techniques such as matched filter (MF), minimum variance distortionless response (MVDR), and multiple signal classification (MUSIC) were compared and evaluated. The result shows that MUSIC comes out as giving the best ranging performance of all.

As multipath are present in the channel model, the signals are also highly correlated between the desired signals and the interference signals. Therefore, forward-backward smoothing is implemented in combination with MUSIC to identify a higher number of correlated signals and to improve the ranging resolution.

MUSIC is a subspace-based DOA estimation method which divides the vector space into a signal subspace and noise subspace. Exact knowledge of estimating the number of signals is necessary to be able to distinguish between noise and signal subspace. Consequently, MUSIC is also known to be able to perform best with precise information on the number of sources. The number of sources, in this case, is the number of separable multipath of the channel model. In the earlier simulations, this number of separable multipath was assumed to be half of the highest possible number of total multipath. An information theory based algorithm, Akaike information criterion - minimum descriptive length (AIC-MDL), has been investigated in this thesis in combination with MUSIC and forward-backward smoothing to improve the ranging accuracy. The number of separable multipath is estimated using AIC-MDL algorithm so that it can further diminish the disturbance from multipath issues.

Chapter 4 focuses on reducing the result of ranging bias from Chapter 3. The first part of this chapter suggests that bias compensation is possible to improve the ranging precision given the right information of channel parameter values. The second part of the chapter concentrates on problems of estimating the bias value given specific knowledge of channel parameter values. Bias value estimation for various situations of an indoor environment were analysed and stored. It is done by simulating several channel parameters, such as K-Factor, signal to noise ratio (SNR), ray interval rate (λ), and ray decay constant (γ) with different a range of values. The results reveal

K-factor and SNR as the two main parameters that are crucial in contributing to the bias and need to be estimated in order to lookup the estimation of ranging bias value. Estimation of K-Factor and SNR has been discussed by Ramesh et al. in [36] and Abdi et al. in [37], respectively. The results in Chapter 4 have shown that bias compensation with exact estimation of channel parameter value can further reduce the absolute bias value until up an order of magnitude.

Chapter 5 focuses on using another variation of ranging method based on two main factors: improvement of ranging performance over low SNR and avoid estimating the number of signals while still maintaining the ranging performance. As shown in Chapter 4, SNR is an essential parameter along with K-Factor that affects the ranging performance of AIC-MDL. Performance of AIC-MDL is known to degrade severely over low SNR which could affect the overall ranging performance. The MUSIC-like algorithm is proposed to improve the result over poor SNR conditions without estimating the number of separable multipath. The results show that the estimation accuracy of MUSIC-like is similar to AIC-MDL over high SNR conditions. The ranging performance also improves over the existing model order estimation methods under adverse SNR environments.

6.2 Future Works

In this section, several recommendations and challenges for extending this research are presented:

- **Testing algorithms on real measurements**

  Channel modelling and simulation in this thesis were performed using MATLAB software. It is vital to check further the advantages of all the proposed approaches using real indoor measurement. Also, these measurements could result in new challenges, such as the possibility of some information loss between each transceiver.

- **Reducing the number of tones**

  The number of tones used in this thesis equals K_f as explained in Chapter 2. It is interesting to see if the measurement can be done with fewer tones and check the trade-offs between reducing the number of tones and the ranging accuracy. Compressed sensing (CS) is one of the possible methods to do this if the channel vector $\mathbf{h}$ is N-sparse, with $N < K_f$ [46, 47].

- **Optimal tone placement**

  In this thesis, several ranging algorithms are derived and combined with a bias compensation in order to improve the ranging results in the ISM band. However, the exact knowledge of channel state information (CSI) is fundamental to perform all of these approaches above [48]. Currently, the channel estimation to obtain CSI is done by using K_f tones in a conventional uniform pattern. Non-uniform placement tones can be considered in order to find the most optimal placement tones.

- **Reducing the computational complexity of the MUSIC-Like algorithm** The MUSIC-Like method requires a high computational time to find an eigenvector related to the minimum eigenvalue of the matrix depending on each delay and the correlation matrix of the steering vector, or called as minor component [49, 50]. A statistical method to extract this component adaptively, such as minor component analysis (MCA) can be considered to solve a generalized eigen-decomposition problem [51]. Recently, Samir et al. [52] introduce a fast MCA algorithm to reduce the computational time further.

Appendix A

In this appendix, Figure A.1, A.2, and A.3 presented the example pseudo-spectrum results of MUSIC + Smoothing for the thesis case studies with different size of Hankel matrix **H**.

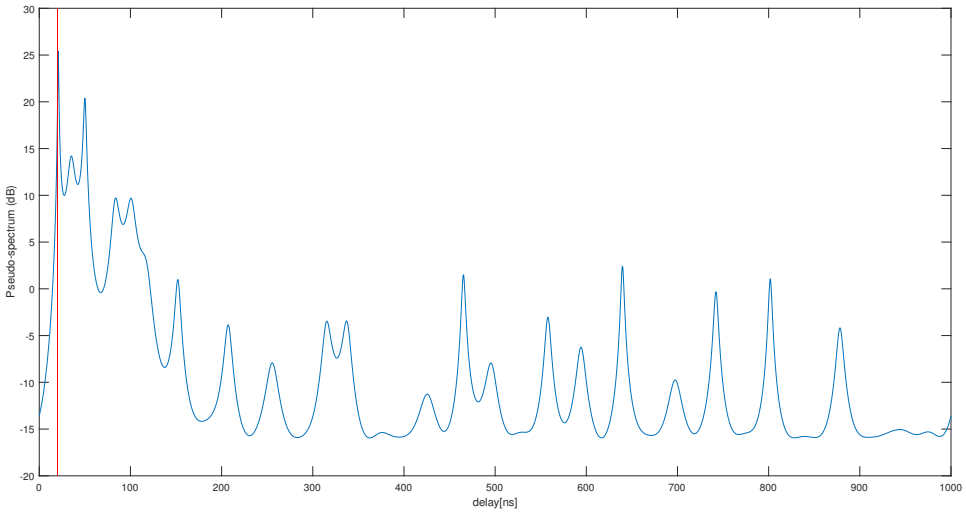

Figure A.1: An example of pseudo-spectrum of MUSIC + Smoothing with **H** size of 41×40

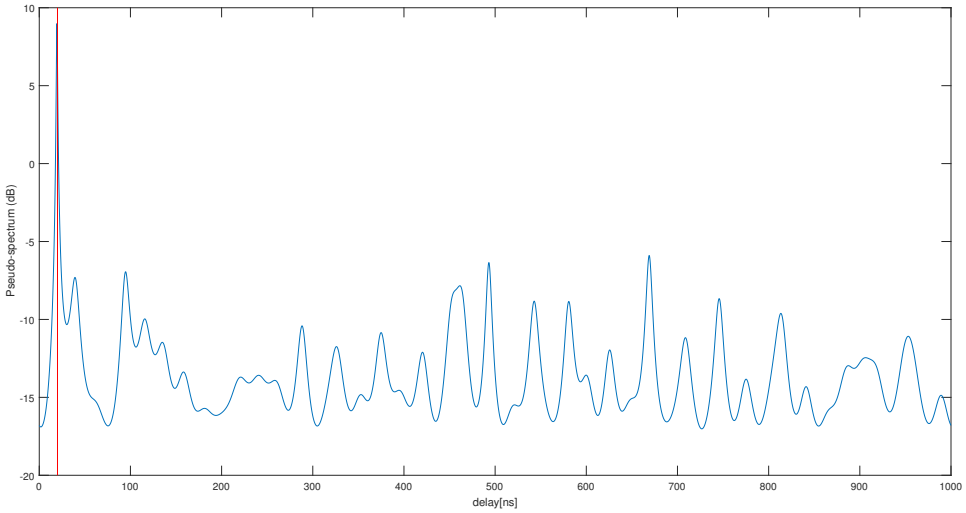

Figure A.2: An example of pseudo-spectrum of MUSIC + Smoothing with $\mathbf{H}$ size of 54×27

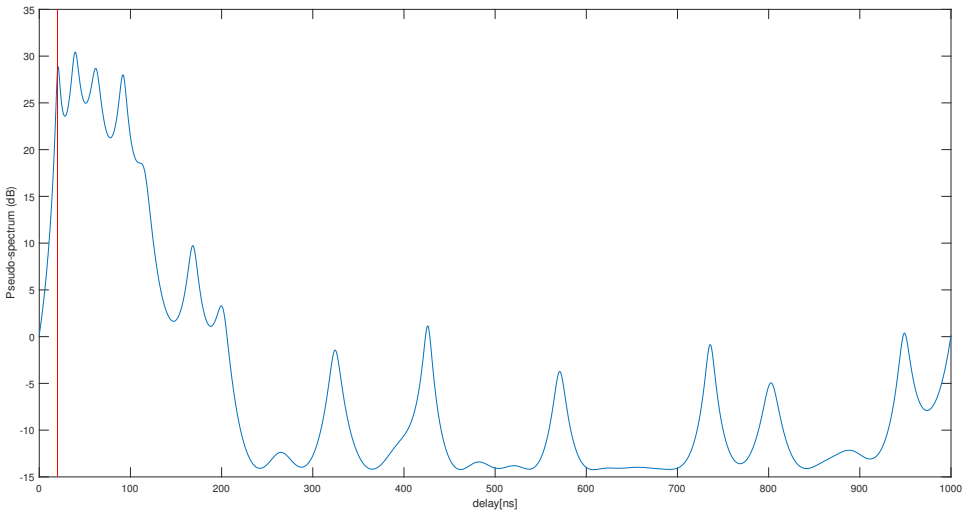

Figure A.3: An example of pseudo-spectrum of MUSIC + Smoothing with $\mathbf{H}$ size of 27×54

Appendix B

In this appendix, the performance data for various ranging algorithms are presented in Table B.1 - B.4.

Table B.1: Results of ranging bias

	Matched Filter	MVDR	MUSIC	AIC-MDL	MUSIC-Like
MIN [m]	-5.945	-5.854	-1.349	-1.221	-1.678
MAX [m]	11.671	15.187	6.617	4.255	1.599
MEAN [m]	0.745	0.107	0.117	0.086	-0.007
MEDIAN [m]	0.446	0.079	0.098	0.079	-0.012
STD [m]	1.400	0.745	0.491	0.344	0.463
10% PERCENTILE [m]	-0.378	-0.362	-0.250	-0.287	-0.461
90% PERCENTILE [m]	2.094	0.537	0.519	0.409	0.394

Table B.2: Results of MUSIC + Smoothing ranging bias

	MUSIC 41×40	MUSIC 54×27	MUSIC 27×54
MIN [m]	-1.349	-2.283	-1.825
MAX [m]	6.617	13.117	8.631
MEAN [m]	0.117	0.126	0.188
MEDIAN [m]	0.098	0.116	0.116
STD [m]	0.491	0.645	0.594
10% PERCENTILE [m]	-0.250	-0.235	-0.342
90% PERCENTILE [m]	0.519	0.427	0.501

Table B.3: Results of MUSIC + Forward-Backward Smoothing ranging bias

	MUSIC 41×40	MUSIC 54×27	MUSIC 27×54	FBS 41×40	FBS 27×54	FBS 54×27
MIN [m]	-1.349	-2.283	-1.825	-5.744	-3.418	-1.514
MAX [m]	6.617	13.117	8.631	2.771	4.035	4.566
MEAN [m]	0.117	0.126	0.188	0.061	0.061	0.143
MEDIAN [m]	0.098	0.116	0.116	0.061	0.061	0.116
STD [m]	0.491	0.645	0.594	0.402	0.481	0.436
10% PERCENTILE [m]	-0.342	-0.342	-0.268	-0.268	-0.360	-0.250
90% PERCENTILE [m]	0.519	0.519	0.557	0.391	0.501	0.519

Table B.4: Results of MUSIC + Forward-Backward Smoothing + AIC MDL ranging bias

	MUSIC 41×40	MUSIC 54×27	MUSIC 27×54	FBS 41×40	FBS 54×27	FBS 27×54	AIC-MDL 41×40	AIC-MDL 54×27	AIC-MDL 27×54
MIN [m]	-1.349	-2.283	-1.825	-5.744	-3.418	-1.514	-1.221	-1.825	-1.129
MAX [m]	6.617	13.117	8.631	2.771	4.035	4.566	4.255	13.850	2.552
MEAN [m]	0.117	0.126	0.188	0.061	0.061	0.143	0.086	0.102	0.176
MEDIAN [m]	0.098	0.116	0.116	0.061	0.061	0.116	0.079	0.061	0.153
STD [m]	0.491	0.645	0.594	0.402	0.481	0.436	0.344	0.692	0.329
10% PERCENTILE [m]	-0.342	-0.342	-0.268	-0.268	-0.360	-0.250	-0.287	-0.342	-0.177
90% PERCENTILE [m]	0.519	0.519	0.557	0.391	0.501	0.519	0.409	0.501	0.556

Appendix C

In this appendix, Table C.1 indicates the performance data of bias compensation for different ranging algorithms, derived from Table B.4. Table C.2 - C.7 depicts the performance of bias compensation for different radio environments. $N_s = \frac{L+1}{2}$

Table C.1: Results of ranging bias before and after compensation

	Before Bias Compensation			After Bias Compensation		
	MUSIC 41×40	**FBS 41×40**	**AIC-MDL 41×40**	**MUSIC 41×40**	**FBS 41×40**	**AIC-MDL 41×40**
MIN [m]	-1.349	-5.744	-1.221	-3.345	-5.451	-1.166
MAX [m]	6.617	2.771	4.255	3.284	1.874	2.625
MEAN [m]	0.117	0.061	0.086	-0.025	-0.016	0.016
MEDIAN [m]	0.098	0.061	0.079	-0.030	-0.012	0.025
STD [m]	0.491	0.402	0.344	0.425	0.464	0.310
10% PERCENTILE [m]	-0.342	-0.268	-0.287	-0.452	-0.378	-0.323
90% PERCENTILE [m]	0.519	0.391	0.489	0.391	0.336	0.318

Table C.2: Ranging bias for different K-factor and ray interval rate (Λ) [m]

Λ [1/ns] \ K-factor	**0.1**	**0.2**	**0.3**	**0.4**	**0.5**	**0.6**	**0.7**	**0.8**	**0.9**	**1**
0.1	0.354	0.171	0.153	0.080	0.080	0.061	0.061	0.043	0.043	0.052
0.2	0.519	0.327	0.226	0.153	0.134	0.134	0.098	0.098	0.080	0.080
0.3	0.519	0.354	0.226	0.208	0.189	0.134	0.116	0.116	0.098	0.098
0.4	0.556	0.391	0.263	0.208	0.171	0.153	0.134	0.134	0.098	0.080
0.5	0.592	0.372	0.281	0.226	0.189	0.134	0.116	0.098	0.098	0.089
0.6	0.574	0.391	0.299	0.244	0.189	0.171	0.116	0.134	0.098	0.080
0.7	0.574	0.391	0.299	0.226	0.189	0.171	0.134	0.116	0.134	0.098
0.8	0.592	0.425	0.263	0.208	0.189	0.171	0.134	0.134	0.098	0.116
0.9	0.620	0.409	0.299	0.244	0.208	0.144	0.134	0.116	0.116	0.098
1	0.610	0.391	0.290	0.226	0.189	0.153	0.116	0.116	0.116	0.116

Table C.3: Ranging bias for different K-factor and Λ after compensation [m]

Λ [1/ns] \ K-factor	**0.1**	**0.2**	**0.3**	**0.4**	**0.5**	**0.6**	**0.7**	**0.8**	**0.9**	**1**
0.1	-0.037	0	-0.037	0.018	0	0.019	-0.018	0.018	0	-0.009
0.2	0.037	-0.01	0.018	0.018	0.019	0	0.018	-0.019	0.018	-0.019
0.3	0.073	0	0.037	0.036	-0.018	0	0.018	-0.018	-0.019	0
0.4	0.036	0	0.018	0	0	0.009	0	0	0	0.018
0.5	0	0	0	-0.018	-0.018	0.019	0.018	0.036	0	0.009
0.6	0.055	0.018	-0.018	0	0	0.018	0.037	-0.009	0.018	0
0.7	0.082	0.018	0.019	0.018	0.018	-0.018	0	0	-0.018	0
0.8	0.037	-0.034	0.036	0.018	0	-0.018	0	0.019	0.018	0
0.9	0.027	0	0	0	0	0.027	0.019	0	0.018	-0.019
1	-0.018	0.018	0.009	0.037	0	0	0.037	0	0	-0.018

Table C.4: Ranging bias for different K-factor and SNR [m]

K-factor \ SNR [dB]	**11**	**12**	**13**	**14**	**15**	**16**	**17**	**18**	**19**	**20**
0.1	0.904	0.94	0.766	0.702	0.72	0.684	0.629	0.611	0.556	0.537
0.2	0.592	0.565	0.519	0.482	0.446	0.446	0.446	0.373	0.391	0.373
0.3	0.427	0.464	0.373	0.382	0.318	0.299	0.308	0.299	0.226	0.263
0.4	0.336	0.318	0.281	0.263	0.244	0.226	0.244	0.244	0.208	0.189
0.5	0.299	0.281	0.263	0.244	0.226	0.208	0.189	0.153	0.171	0.171
0.6	0.263	0.244	0.226	0.199	0.189	0.171	0.171	0.153	0.153	0.134
0.7	0.244	0.226	0.171	0.18	0.171	0.153	0.153	0.171	0.134	0.134
0.8	0.189	0.171	0.153	0.171	0.153	0.116	0.116	0.098	0.116	0.098
0.9	0.189	0.171	0.153	0.153	0.116	0.134	0.134	0.116	0.098	0.116
1	0.153	0.153	0.134	0.098	0.116	0.116	0.098	0.116	0.08	0.08

Table C.5: Ranging bias for different K-factor and SNR after compensation [m]

K-factor \ SNR [dB]	**11**	**12**	**13**	**14**	**15**	**16**	**17**	**18**	**19**	**20**
0.1	-0.037	-0.073	0.028	0.018	0.055	-0.019	0.018	0.009	0.036	0.055
0.2	0.028	-0.009	0	0.019	0	-0.019	-0.037	0.018	-0.037	-0.055
0.3	0	-0.073	0.018	-0.046	0.018	0.009	0	-0.018	0.055	-0.037
0.4	0.027	0.018	0.018	0.036	0.019	0.037	0	0	0	0
0.5	0	0.018	-0.01	-0.018	0	0	0	0	0	-0.018
0.6	0	-0.018	-0.037	0.009	0	0.018	0.018	0	-0.019	-0.018
0.7	0	0.018	0.037	0.009	0	0	0	0	0	-0.018
0.8	0	0.018	0	0	-0.019	0.037	0.036	0.036	0	-0.019
0.9	-0.018	-0.018	0	0	0.037	0	-0.036	-0.009	-0.019	-0.037
1	0.018	0	0.019	0.055	0	-0.018	0	0	0.018	0

Table C.6: Ranging bias for different K-factor and ray decay factor (γ) [m]

K-factor \ γ [dB/ns]	**0.01**	**0.02**	**0.03**	**0.04**	**0.05**	**0.06**	**0.07**	**0.08**	**0.09**	**0.1**
0.1	0.556	0.556	0.574	0.556	0.574	0.592	0.556	0.537	0.537	0.574
0.2	0.391	0.336	0.345	0.354	0.354	0.336	0.336	0.354	0.373	0.318
0.3	0.208	0.281	0.263	0.235	0.263	0.244	0.263	0.263	0.244	0.244
0.4	0.189	0.189	0.199	0.226	0.171	0.208	0.208	0.171	0.208	0.189
0.5	0.153	0.171	0.153	0.171	0.153	0.153	0.153	0.153	0.171	0.171
0.6	0.116	0.134	0.134	0.134	0.134	0.134	0.153	0.153	0.116	0.153
0.7	0.134	0.116	0.098	0.107	0.116	0.098	0.116	0.116	0.116	0.116
0.8	0.098	0.116	0.116	0.098	0.098	0.098	0.098	0.098	0.116	0.098
0.9	0.098	0.116	0.098	0.098	0.098	0.098	0.098	0.08	0.116	0.098
1	0.08	0.08	0.08	0.08	0.08	0.08	0.06	0.08	0.08	0.08

Table C.7: Ranging bias for different K-factor and γ after compensation [m]

K-factor \ γ [dB/ns]	**0.01**	**0.02**	**0.03**	**0.04**	**0.05**	**0.06**	**0.07**	**0.08**	**0.09**	**0.1**
0.1	0.036	-0.019	0	-0.01	-0.037	-0.073	-0.037	0.019	0.019	0
0.2	-0.074	0.018	0.009	0	0	-0.037	0	-0.018	0	0.018
0.3	0.018	-0.018	0	-0.009	-0.019	-0.018	0	-0.019	0	0.019
0.4	0	0	-0.01	0	0.037	-0.037	-0.019	0.018	-0.019	0
0.5	0	0	0.018	-0.018	0.018	0	0.018	0	-0.018	0
0.6	0	0	0	0	0.019	0	-0.019	-0.019	0.018	0
0.7	-0.018	-0.018	0.018	-0.009	0	0.018	0	0	0.018	0
0.8	-0.019	0	-0.018	0	0.018	0	0.018	0.018	-0.037	0
0.9	-0.019	-0.018	0	0	-0.019	-0.019	0.009	0	0	0
1	0	0	0.018	0	0.018	0.018	0.038	0.018	-0.019	0.009

Bibliography

[1] M. Wehner, R. Richter, S. Zeisberg, and O. Michler, "High resolution approach for phase based TOF ranging using compressive sampling," in *2011 8th Workshop on Positioning, Navigation and Communication*. IEEE, Apr. 2011.

[2] W. Kluge and D. Eggert. (2009, Sep.) Ranging with IEEE 802.15.4 Narrow-Band PHY. Atmel. [Online]. Available: https://mentor.ieee.org/802.15/dcn/09/15-09-0613-01-004f-ranging-with-ieee-802-15-4-narrow-band-phy.ppt

[3] Y. Gu, A. Lo, and I. Niemegeers, "A survey of indoor positioning systems for wireless personal networks," *IEEE Communications Surveys & Tutorials*, vol. 11, no. 1, pp. 13–32, 2009.

[4] B. Hofmann-Wellenhof, H. Lichtenegger, and J. Collins, *Global Positioning System*. Springer Vienna, 2001.

[5] H. Liu, H. Darabi, P. Banerjee, and J. Liu, "Survey of wireless indoor positioning techniques and systems," *IEEE Transactions on Systems, Man and Cybernetics, Part C (Applications and Reviews)*, vol. 37, no. 6, pp. 1067–1080, Nov. 2007.

[6] G. Shen, R. Zetik, H. Yan, O. Hirsch, and R. S. Thoma, "Time of arrival estimation for range-based localization in UWB sensor networks," in *2010 IEEE International Conference on Ultra-Wideband*. IEEE, Sep. 2010.

[7] R. Pe and M. Sichitiu, "Angle of arrival localization for wireless sensor networks," in *2006 3rd Annual IEEE Communications Society on Sensor and Ad Hoc Communications and Networks*. IEEE, 2006.

[8] T. Kikuzuki, A. Wada, M. Hamaminato, and T. Ninomiya, "Automatic standard classification method for the 2.4 GHz ISM band," in *2017 IEEE 85th Vehicular Technology Conference (VTC Spring)*. IEEE, Jun. 2017.

[9] C. Falsi, D. Dardari, L. Mucchi, and M. Z. Win, "Time of arrival estimation for UWB localizers in realistic environments," *EURASIP Journal on Advances in Signal Processing*, vol. 2006, no. 1, jul 2006.

[10] F. Nekoogar, *Ultra-Wideband Communications: Fundamentals and Applications: Fundamentals and Applications*. Prentice Hall, 2005.

[11] S. O. Rice, "Statistical properties of a sine wave plus random noise," *Bell System Technical Journal*, vol. 27, no. 1, pp. 109–157, Jan. 1948.

[12] J. Proakis and M. Salehi, *Digital Communications*. McGraw-Hill Education - Europe, 2007.

[13] G. Turin, F. Clapp, T. Johnston, S. Fine, and D. Lavry, "A statistical model of urban multipath propagation," *IEEE Transactions on Vehicular Technology*, vol. 21, no. 1, pp. 1–9, Feb. 1972.

[14] R. Ganesh and K. Pahlavan, "Statistical modelling and computer simulation of indoor radio channel," *IEE Proceedings I Communications, Speech and Vision*, vol. 138, no. 3, p. 153, 1991.

[15] T. Rappaport, S. Seidel, and K. Takamizawa, "Statistical channel impulse response models for factory and open plan building radio communicate system design," *IEEE Transactions on Communications*, vol. 39, no. 5, pp. 794–807, may 1991.

[16] H. Hashemi, "The indoor radio propagation channel," *Proceedings of the IEEE*, vol. 81, no. 7, pp. 943–968, jul 1993.

[17] A. Saleh and R. Valenzuela, "A statistical model for indoor multipath propagation," *IEEE Journal on Selected Areas in Communications*, vol. 5, no. 2, pp. 128–137, Feb. 1987.

[18] K. Pahlavan and A. H. Levesque, *Wireless Information Networks*. John Wiley & Sons Inc, 2005.

[19] H. Nikookar and R. Prasad, *Introduction to Ultra Wideband for Wireless Communications*, 1st ed., ser. Signals and Communication Technology. Springer Netherlands, 2009.

[20] W. Liao and A. Fannjiang, "MUSIC for single-snapshot spectral estimation: Stability and super-resolution," *Applied and Computational Harmonic Analysis*, vol. 40, no. 1, pp. 33–67, Jan. 2016.

[21] T.-J. Shan, M. Wax, and T. Kailath, "On spatial smoothing for direction-of-arrival estimation of coherent signals," *IEEE Transactions on Acoustics, Speech, and Signal Processing*, vol. 33, no. 4, pp. 806–811, Aug. 1985.

[22] J. Evans, J. Johnson, and D. Sun, "Application of advanced signal processing techniques to angle of arrival estimation in ATC navigation and surveillance systems," Massachusetts Imtitute of Technology Lincoln Laboratory, Lexington, Massachusetts, techreport 582, Jun. 1982. [Online]. Available: http://hdl.handle.net/1721.1/97639

[23] T.-J. Shan and T. Kailath, "Adaptive beamforming for coherent signals and interference," *IEEE Transactions on Acoustics, Speech, and Signal Processing*, vol. 33, no. 3, pp. 527–536, Jun. 1985.

[24] M. S. Bartlett, "Smoothing periodograms from time-series with continuous spectra," *Nature*, vol. 161, no. 4096, pp. 686–687, May 1948.

[25] ——, "Periodogram analysis and continuous spectra," *Biometrika*, vol. 37, no. 1/2, p. 1, Jun 1950.

[26] J. Capon, "High-resolution frequency-wavenumber spectrum analysis," *Proceedings of the IEEE*, vol. 57, no. 8, pp. 1408–1418, 1969.

[27] R. Schmidt, "Multiple emitter location and signal parameter estimation," *IEEE Transactions on Antennas and Propagation*, vol. 34, no. 3, pp. 276–280, Mar. 1986.

[28] R. T. Williams, S. Prasad, A. K. Mahalanabis, and L. H. Sibul, "An improved spatial smoothing technique for bearing estimation in a multipath environment," *IEEE Transactions on Acoustics, Speech, and Signal Processing*, vol. 36, no. 4, pp. 425–432, Apr 1988.

[29] M. Wax and T. Kailath, "Detection of signals by information theoretic criteria," *IEEE Transactions on Acoustics, Speech, and Signal Processing*, vol. 33, no. 2, pp. 387–392, Apr 1985.

[30] H. Akaike, "A new look at the statistical model identification," *IEEE Transactions on Automatic Control*, vol. 19, no. 6, pp. 716–723, Dec. 1974.

[31] J. Rissanen, "Modeling by shortest data description," *Automatica*, vol. 14, no. 5, pp. 465–471, Sep. 1978.

[32] T. W. Anderson, "Asymptotic theory for principal component analysis," *The Annals of Mathematical Statistics*, vol. 34, no. 1, pp. 122–148, Mar. 1963.

[33] H. L. V. Trees, *Optimum Array Processing*. John Wiley & Sons, Inc., Mar. 2002.

[34] G. Schwarz, "Estimating the dimension of a model," *The Annals of Statistics*, vol. 6, no. 2, pp. 461–464, Mar 1978.

[35] G. Xu, R. Roy, and T. Kailath, "Detection of number of sources via exploitation of centro-symmetry property," *IEEE Transactions on Signal Processing*, vol. 42, no. 1, pp. 102–112, 1994.

[36] A. Ramesh, A. Chockaligam, and L. Milstein, "SNR estimation in generalized fading channels and its application to turbo decoding," in *ICC. International Conference on Communications*. IEEE, Jun. 2001.

[37] A. Abdi, C. Tepedelenlioglu, M. Kaveh, and G. Giannakis, "On the estimation of the K parameter for the rice fading distribution," *IEEE Communications Letters*, vol. 5, no. 3, pp. 92–94, Mar. 2001.

[38] P. Djuric, "A model selection rule for sinusoids in white gaussian noise," *IEEE Transactions on Signal Processing*, vol. 44, no. 7, pp. 1744–1751, Jul. 1996.

[39] Y. Zhang and B. P. Ng, "MUSIC-like DOA estimation without estimating the number of sources," *IEEE Transactions on Signal Processing*, vol. 58, no. 3, pp. 1668–1676, Mar. 2010.

[40] V. V. Reddy, B. P. Ng, and A. W. H. Khong, "Insights into MUSIC-like algorithm," *IEEE Transactions on Signal Processing*, vol. 61, no. 10, pp. 2551–2556, May 2013.

[41] M. W. Trevor Hastie, Robert Tibshirani, *Statistical Learning with Sparsity*. Taylor & Francis Inc., 2015.

[42] B. N. Parlett, *The Symmetric Eigenvalue Problem (Classics in Applied Mathematics)*. Society for Industrial and Applied Mathematics, 1987.

[43] Y. Saad, *Numerical Methods for Large Eigenvalue Problems*. Society for Industrial and Applied Mathematics, 2011.

[44] J. Sherman and W. J. Morrison, "Adjustment of an inverse matrix corresponding to a change in one element of a given matrix," *The Annals of Mathematical Statistics*, vol. 21, no. 1, pp. 124–127, Mar. 1950.

[45] M. S. Bartlett, "An inverse matrix adjustment arising in discriminant analysis," *The Annals of Mathematical Statistics*, vol. 22, no. 1, pp. 107–111, Mar. 1951.

[46] D. Donoho, "Compressed sensing," *IEEE Transactions on Information Theory*, vol. 52, no. 4, pp. 1289–1306, Apr. 2006.

[47] E. Candes, J. Romberg, and T. Tao, "Robust uncertainty principles: exact signal reconstruction from highly incomplete frequency information," *IEEE Transactions on Information Theory*, vol. 52, no. 2, pp. 489–509, Feb. 2006.

[48] I. Barhumi, G. Leus, and M. Moonen, "Optimal training design for MIMO OFDM systems in mobile wireless channels," *IEEE Transactions on Signal Processing*, vol. 51, no. 6, pp. 1615–1624, Jun. 2003.

[49] F.-L. Luo, R. Unbehauen, and A. Cichocki, "A minor component analysis algorithm," *Neural Networks*, vol. 10, no. 2, pp. 291–297, Mar. 1997.

[50] E. Oja, "Principal components, minor components, and linear neural networks," *Neural Networks*, vol. 5, no. 6, pp. 927–935, Nov. 1992.

[51] Q. Zhang and Y.-W. Leung, "A class of learning algorithms for principal component analysis and minor component analysis," *IEEE Transactions on Neural Networks*, vol. 11, no. 2, pp. 529–533, Mar. 2000.

[52] S. Attallah and K. Abed-Meraim, "A fast adaptive algorithm for the generalized symmetric eigenvalue problem," *IEEE Signal Processing Letters*, vol. 15, pp. 797–800, 2008.

[53] C. Gentile, N. Alsindi, R. Raulefs, and C. Teolis, *Geolocation Techniques*. Springer New York, 2013.